Detectors for the SSC: Summary Report

H. H. Williams
Physics Department, University of Pennsylvania
Philadelphia, Pennsylvania 19104

SUMMARY

A review is presented of the major considerations for detectors at the SSC. Particular emphasis is placed on the design of a large 4 π magnetic detector and on the feasibility of building such a detector. The results of each of the Working Groups are summarized. It appears to be possible to build a detector that incorporates nearly all of the desired features, but significant R & D on detectors particularly in the area of electronics, will be required.

INTRODUCTION

In discussing detectors and instrumentation for the SSC at the 1986 Snowmass Workshop, one of the first questions which arose was how one could best progress beyond the work accomplished at the 1984 Snowmass summer study[1], at workshops for detectors at the LHC[2], and at various intervening workshops aimed at studying the physics capabilities of the SSC. During these studies considerable progress has been made on outlining the required characteristics of detectors: the desired thickness, segmentation, and energy resolution of the calorimeters; the number of wires and cell size for tracking, as dictated by considerations of instantaneous rate and radiation damage; the triggering rate and momentum resolution for muons; questions of electron identification, etc. In addition, a certain amount of brainstorming has taken place concerning different types of large 4 π detectors: for example, magnetic vs. non-magnetic, detectors built with "conventional" technology vs. those which might be built with new technology, specialized detectors which emphasize muon detection (generally at the risk of somewhat inferior detection of electrons and jets) vs. detectors which are designed with more or less equal priority assigned to the detection of electrons, muons, and jets of particles. Such considerations of the optimal conceptual design for a detector are far from exhausted and could well have been one of the primary topics for Snowmass '86. It was decided instead to adopt, for the purpose of this workshop, one of the commonly accepted conceptual designs for a large 4 π detector with solenoidal field and to evaluate in some detail whether one could realistically build such a detector. The motivations were twofold: first, very little consideration has been given in previous studies to the question of whether it is feasible to realistically build such a detector. Second, it was felt that a more detailed consideration of such a detector might sharpen one's perception of the various R & D topics which must be pursued particularly aggressively.

The discussion below presents first the overview of the detector considered, and then discusses in greater detail each of the subsystems. In addition to presenting the design considered, with some discussion as to why it was chosen, considerable emphasis is placed on progress since the Snowmass '84 workshop and on those R & D topics which seemed to the participants to be of particular importance. Needless to say, the list of topics is not complete nor has any significant effort been made to rank them in order of importance.

CONCEPTUAL DESIGN

The design goals for a large 4π detector, chosen on the basis that the detector should allow one to effectively address a wide range of the physics processes of greatest interest, include:

* hermetic calorimeter coverage over the rapidity range of at least $|y| < 5.5$ in order to permit accurate measurement of missing transverse energy.
* measurement capability of jet energies up to the multi-TeV range with good energy resolution.
* optimized efficiency for multi-jet detection and mass reconstruction of particles decaying into jets or jets and leptons.
* detection of muons over the rapidity range $|y| < 5$ with the ability to determine, at least crudely, muon momenta at the trigger level over much of the same rapidity interval
* optimal detection and identification of electrons via calorimetry in conjunction with tracking or other devices
* momentum measurement capability for charged tracks in the central rapidity interval $|y| < 2$, i.e. a magnetic detector
* precision secondary vertex detection in at least the central rapidity interval for flavor tagging and the detection of relatively long-lived states
* some sensitivity to exotic new particles beyond a missing energy signature
* capability of operation at the SSC design luminosity (10^{33} $cm^{-2}sec^{-1}$) and at lower luminosities if desirable.

Conceptual designs of detectors to meet these goals have been put forth, among other places, in the Snowmass 84 workshop[1] and in the DCMAP report[4]. The 4π Group at this workshop examined the two designs discussed in the latter reference and concluded that they were representative of the general problems posed by a 4π magnetic detector; they therefore decided to examine these designs critically with regard to overall feasibility, servicability, and systems level performance. No real attempt was made to determine a new or "better" design.

Each of the two designs, schematically shown in Figures 1 and 2, utilize the following features:

1. uranium liquid-argon (or lead liquid-argon) calorimetry for the first 5-6 absorption lengths (the precision calorimeter)

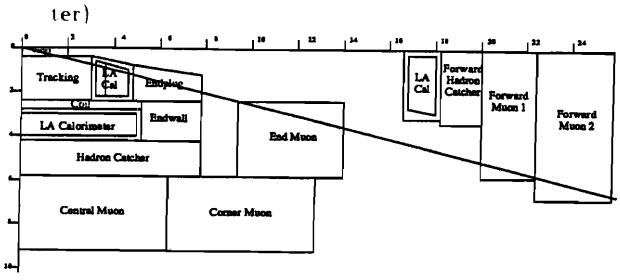

Figure 1a
A plan view of Detector B arranged along the beamline with all elements positioned for data taking.

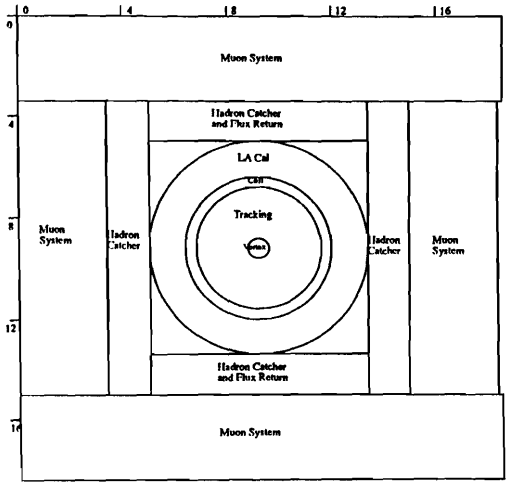

Figure 1b
An end view of the central region of Detector B showing space allocation of the various systems as a function of radius.

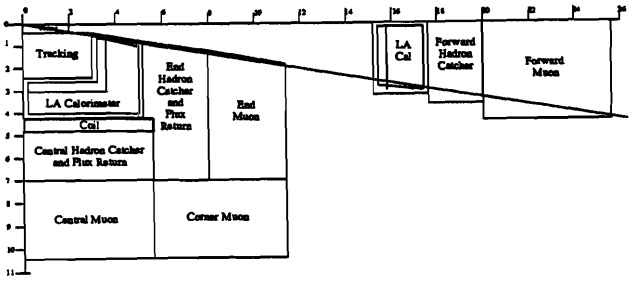

Figure 2
A plan view of Detector A arranged along the beamline with all elements in position for data taking.

2. "conventional" drift chambers or proportional drift tubes for the central tracking

3. superconducting solenoid to provide the magnetic field in the central region

4. a return yoke instrumented with wire chambers with pad readout to provide an additional 6 absorption lengths of lower precision "tail catcher" calorimetry

5. a massive, magnetized iron muon detection and measurement system

The solenoidal field orientation was chosen primarily because it provides more uniform coverage in the central region (where the highest mass events are preferentially produced) and because it provides the simplest triggers on transverse momentum. However, a more detailed comparison of the relative merits of solenoid and dipole fields is certainly warranted. The primary difference between the two designs considered here lies in the choice of whether the precision calorimeter is placed inside, or outside, the magnet coil.

Since various other working groups addressed the calorimetery, tracking, etc. in detail, the 4 π group concentrated on understanding design problems at the level of the overall detector.[3] These include ensuring that the various detector components fit together, that they can be moved in such a way as to allow periodic access to each system, and that it is possible to route the cables out of the detector. Realistic estimates were made of the space required for cryostats, cables, etc.

Of particular concern was the impact of the cryostats and cable plant on the hermeticity of the calorimeter. Figure 3 illustrates the region of nonuniform response that can be expected due to coil and cryostats for the geometry in which the bulk of the calorimeter is outside the magnetic field. For the case of the precision calorimeter inside the magnetic field a somewhat radical approach was considered, that of dividing the calorimeter, and the solenoid, in the center (Figure 4). The motivation was that a nonuniform region of fixed size subtends a smaller region of rapidity if it is placed at 90 degrees than if it is placed near 30 degrees. Some attempt has been made to stagger the calorimeters so that complete coverage is maintained. It is not known whether the resulting configurations are sufficiently hermetic and implementing studies to answer to this question should be a high priority.

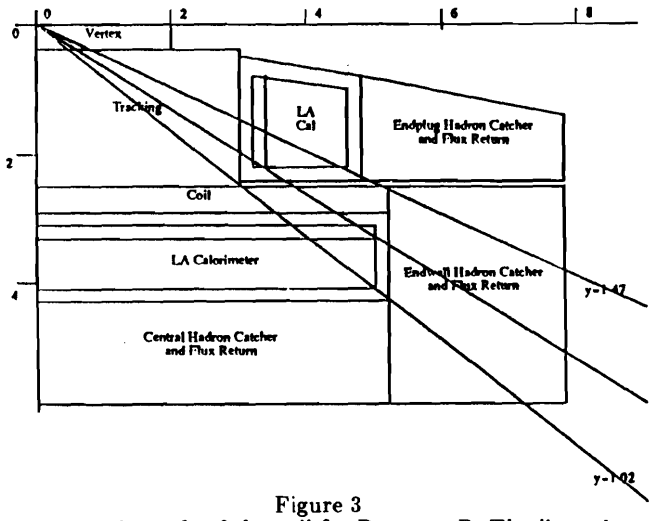

Figure 3
A crack at the ends of the coil for Detector B. The lines show the region of degraded calorimetry.

CALORIMETRY

The conceptual design of the calorimetry follows in a fairly straightforward way from the requirement that one be able to detect efficiently, and with as high a rejection of backgrounds as is possible, electrons, neutrinos (and other weakly interacting particles), quarks and gluons, W's and Z's. One of the most challenging goals for the calorimetry is that one be able to identify the $W \rightarrow q\bar{q}$ and $Z \rightarrow q\bar{q}$ decay modes.

Thickness The overall thickness of the calorimeter is set both by the desire to obtain rather good energy resolution (of order a few percent) for jets in the several TeV range and by the requirement of optimal missing E_t resolution. Extrapolation of existing measurements indicate that to contain 98% of the energy of a 1 TeV hadron requires a calorimeter thickness of 12 absorption lengths. It should be noted however that measurements by different groups of the thickness required for containment of 98 or 99% of the energy of a hadron shower are not in very good agreement with one another[5]. Better measurements will be required before the thickness can be optimized. In the meantime, a thickness of 11-12 λ at 90° and 13-14 λ in the forward direction is typically assumed.

As far as the thickness of the electromagnetic calorimeter is concerned, Monte Carlo studies[6] for the 1984 Workshop indicated that even for an electron of 1 TeV, 26 radiation lengths will contain 98% of the energy; the thickness of the electromagnetic portion of the calorimeter was therefore taken to be 25 X_0

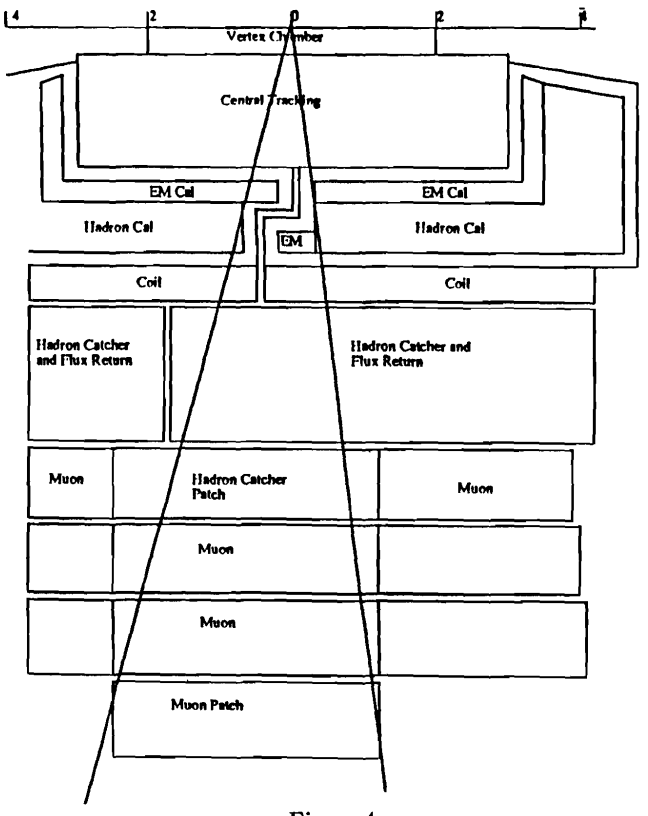

Figure 4
A crack for Detector A at 90°, z = 0, showing a smaller region of degraded calorimetry.

Segmentation The transverse segmentation of the electromagnetic calorimeter is determined both by the necessity for optimal identification of electrons and by the goal of detecting $W \rightarrow q\bar{q}$. Fine segmentation for electron identification is required to reject backgrounds from single hadrons and from single hadrons coincident with photons, and to enable reasonable efficiency for identifying an isolated shower in the high multiplicity environment. While it will be very difficult, if not impossible, to identify electrons arbitrarily close to a jet axis, a study[7] in the 1984 Workshop concluded that top quarks with a transverse momentum of 500 Gev/c could be identified via their semileptonic decays with an efficiency of 80% if the segmentation of the EM calorimeter was $\approx 0.02 \times 0.02$; the efficiency deteriorated significantly for coarser segmentations. Studies of $W \rightarrow q\bar{q}$ decays indicated that a similar segmentation was required if the optimal effective mass resolution were to be obtained; good effective mass resolution for these decays is essential if one is to discriminate effectively against background from ordinary processes[8]. This segmentation corresponds to tower sizes of order $5cm \times 5cm$ in the central region, the largest size compatible with a determination of the shower position to an accuracy of order 2-3 mm. Given these facts, and bearing in mind the desire to keep the number of electronics channels from growing too large, the EM segmentation was assumed to be of order 0.02×0.02 in the central region and of order 0.03×0.03 in the more forward regions of rapidity.

Each EM tower was assumed to be subdivided longitudinally into three sections; a smaller number would probably compromise the electron/pion discrimination given the very large range of electron energies of interest ($\approx$ 30 GeV to 2-3 TeV) and the concomitant change in the shower length. The possibility of reading out the middle longitudinal section with strips rather than pads, in order to improve the position resolution was discussed. While no quantitative study was performed, it was the opinion of the Electron group (based on studies for the D0 detector) that finer segmentation should be in the form of smaller towers (perhaps in only one of the longitudinal sections) rather than strips.[9] An optimization of the segmentation, both longitudinal and transverse, for electron/pion discrimination will probably require additional studies in a test beam.

The segmentation of the hadronic calorimeter in rapidity and ϕ was assumed to be 0.06×0.06. This corresponds to tower sizes somewhat larger than the shower size in the central region but very much smaller than the typical spread of the jet. No convincing argument was made to go to finer sizes, and the consensus was that this size would probably be adequate.

Calorimeter Composition If the thickness and segmentation of the calorimeter seem relatively straightforward, its composition is considerably more problematic. Almost all combinations of absorber (Uranium, lead, iron) and sampling technique (scintillator, gas, liquid argon, warm liquid) were considered. The basic criteria were that the chosen technology must support the desired segmentation, must survive the high counting rates and radiation level, and should provide sufficient energy resolution to enable the detection of $H^o \rightarrow WW$ where one of the W's decays semileptonically and one decays to $q\bar{q}$. Several estimates indicate that the energy resolution of calorimeters constructed with iron or copper absorber would be of order 9-11% for 400 Gev jets due to the fact that the electron/pion response is 1.4-1.6 for low energy particles[10]. By contrast, Uranium and lead calorimeters were estimated to have a resolution of order 2-4% under the same conditions.

Scintillators that are relatively radiation hard should, in principle, survive the radiation from interactions in the central region However, in spite of some assurances from the accelerator physicists that radiation from beam loss would be negligible compared to that from interactions, the experience at the Sp$\bar{p}$S convinced most participants that scintillator was a very risky bet. In addition, it is awkward to realize the desired transverse and longitudinal segmentation. Hence, scintillator was not considered very seriously though one could not completely exclude it for the central hadron calorimeter.

Calorimeters which employ sampling with wire chambers or proportional tubes, which we will often refer to simply as gas calorimetry, does enable fine segmentation in both the transverse and longitudinal directions in a simple and straightforward way (by means of pad readout). In addition, it is relatively easy to construct and reasonably inexpensive. Cracks or dead spaces in the calorimetry occupy a rather small fraction of the volume, though they certainly exist. Disadvantages of gas calorimetry include the fact that it is less dense and it yields poorer energy resolution. The gaps between the absorber plates are typically of order 1 cm, though at least one electromagnetic calorimeter has been constructed with gaps as small as 5 mm[11]. The energy resolution is typically 1.5 - 2 times worse for electromagnetic showers and 1.1 - 1.2 times worse for hadronic showers. Of greatest concern, however, are the facts that (1) it is difficult to maintain the mechanical tolerances required for the response to be uniform to 1-2% over the entire calorimeter, (2) the gain will vary with changes in the temperature and pressure, and (3) it is highly unlikely that gas calorimeters will sustain the instantaneous rate and radiation levels in the forward direction. It is possible that each of these concerns can be overcome and dealt with in a satisfactory manner, but at the moment the challenges seem sufficiently difficult that gas calorimetry does not seem a likely candidate for the complete calorimeter system.

In comparison with scintillator and gas sampling, the use of liquid argon has a long list of advantages. The uniformity of response, both as a function of position and as a function of time, is excellent. The goal of a systematic error of 1% should be able to be obtained with a modest amount of effort. There is also no fundamental problem with achieving the degree of segmentation required (but see the discussion of electronics below). Use of lead or uranium as an absorber yields a ratio of electron to pion response of order 1.2 ± 0.1 with the corresponding good energy resolution, typically 12-15%/$\sqrt{E}$ for electrons and 45 - 55%/$\sqrt{E}$ for hadrons. Thus at the present time, a leading candidate for the calorimeter system is liquid argon sampling with lead or uranium plates. The potential problems with hermeticity due to cryostats are of course non-trivial as was discussed above.

Since liquid argon calorimeters are very expensive, and also because of the difficulties of large cryogenic systems, it is cleary advantageous to restrict their size to the smallest value consistent with obtaining the performance required. The disadvantages of gas calorimetry that argue against its use as the primary system, are not as significant if it is employed as a "catcher" system. Thus it was assumed that the first six absorption lengths (including the electromagnetic section) would be composed of a "precision" calorimeter using liquid argon with uranium or lead absorber plates, and that the last six absorption lengths would be composed of a cruder calorimeter employing iron plates (5 - 10 cm in thickness) with gas sampling. The overall characteristics[12] of the calorimeter are summarized in Table 1.

4π Calorimeter Parameters		
Electromagnetic thickness	25 X_0,	$-1\lambda \pm 5X_0$
Precision Hadronic	5λ	
Total Precision EM + Hadr.	6λ	$\pm 1\lambda$
Hadronic tail catcher	6λ	$\pm 1\lambda$
Total	12λ	$\pm 2\lambda$
Transverse Segmentation		
EM $\Delta y \times \Delta\phi$	.03 x .03	$\pm$ .01
Hadronic $\Delta y \times \Delta\phi$	.06 x .06	
Tail Catcher $\Delta y \times \Delta\phi$	.06 x .06	
Longtitudional Segmentation		
EM	3	$\pm$ 1
Hadronic	2	$\pm$ 1
Tail Catcher	2	$\pm$ 1
Electromagnetic Energy Resolution		
	$\sigma/E = -12\%/\sqrt{E}$	$\pm$ 3%

Table 1
Summary of parameters for the calorimeter.

Construction The construction of the precision calorimeter was assumed to be similar to liquid argon calorimeters currently being built (NA34, D0, SLD);[13-15] the plate thickness is set primarily by a compromise between energy resolution, density, and mechanical simplicity. The absorber plates in the electromagnetic section were assumed to be 2 mm uranium (alternately 2 mm lead) while those in the hadronic section were taken to be 6 mm uranium (alternately 12 mm lead). This yields approximately 40 plates for the electromagnetic and 90 plates for the hadronic. The readout is via pads on a 1.6 mm G-10 board in the center of the gap with 2 mm liquid argon on each side. These specifics were important primarily in evaluating the capacitance of each readout channel and the overall thickness of the calorimeter.

If the absorber were chosen to be lead, it is possible that the absorber itself could divided into "tiles" chosen to have transverse dimensions which just correspond to the desired segmentation in rapidity and ϕ[15]. In this case the G-10 board is not necessary and the gap can be thinner. It was noted that this gain approximately compensates for the added thickness of lead required; hence the total thickness of a lead calorimeter with tiles is approximately the same as that of uranium with printed circuit board readout.

Electronics

A question of crucial importance is whether the response of the calorimeter is sufficiently fast to avoid serious problems with pileup, both at the trigger level and in the offline analysis. This question was therefore addressed in considerable detail. Scintillator calorimeters clearly excel in this regard since the use of fast scintillators and the proper choice of wave shifters allow a response time of the order of several tens of nsec. However, as we have already seen, their use is apt to be precluded by the problems with segmentation and radiation hardness.

At first glance liquid argon would seem to be a poor choice since the drift velocity is 200 nsec per mm for pure argon and 100 nsec for argon mixed with 0.5% methane (larger additions of methane begin to degrade the charge collection efficiency). In fact, the problem of response time is nearly identical for all ionization calorimeters whether they employ liquid argon, gas sampling, or warm liquids such as TMP or TMS. (Silicon sampling is an exception however; it is much faster). This is so not only because the drift time is significant in each case, but also because one of the fundamental limitations is the time required to transfer the charge from the detector to the charge preamplifier.

For the simplest configuration, that in which connections are neglected, the response time of the system is simply the capacitance of the detector times the input impedance of the preamplifer. In real systems, however, the capacitance and inductance of the connections can not be neglected. An analysis of the optimization of the entire system, detector, cables, and preamplifer, indicates that the best risetime that can be obtained (without substantially compromising the signal-to-noise) will be of order $t_r \approx 40 nsec \times l$ where l is the length of the cables in meters[16]. Hence, the only way to obtain a fast risetime is to utilize short connections. This strongly suggests placing the preamplifier within the calorimeter, perhaps in the liquid argon. Such a scheme is being utilized for the NA34 experiment at CERN.[13] Alternatively, one may bring the cables directly through the walls of the cryostat, thus resulting in cable lengths of order 1 - 2 m. A significant complication results if the calorimeter is to be located within the magnetic field since it is desirable for reasons of signal to noise to use transformers to match the source capacitance to the input capacitance of the preamplifier. For the electromagnetic towers, with $C_s \approx 5.4nF$, this transformer matching may be ignored with modest (30 - 40%) increase in the noise level, but for the hadronic towers, with $C_s \approx 60nF$, the degradation is far worse. It has also been pointed out that transformers provide excellent protection for the preamplifier in the event of H. V. breakdown, an eventuality which must be allowed for. If the preamplifiers were to be located directly in the liquid, reliable protection would be essential.

Realistic configurations of source capacitance, cables, and preamplifier were considered for both the Model A and Model B detectors; since the former, in which the calorimeter is placed in the magnetic field, is more problematic, we discuss it in some detail.

For the electromagnetic calorimeter, one may achieve a fast response by bringing the cables directly through the cryostat and locating the preamplifiers on the inside wall of the calorime-

ter. In this way cable lengths of 1-2 m may be achieved. Since there exist 170,000 channels for $\eta < 2.5$ this would result in an enormous number of feedthroughs with a correspondingly large heat loss and possible decrease in the integrity of the cryostat. It was therefore suggested that the readout be divided into fast trigger towers, of segmentation $\Delta\eta \times \Delta\phi \approx 0.06 \times 0.06$ and 1 longitudinal segment, and 170,000 slow readout towers with the finer segmentation $0.02 \times 0.02 - 0.03 \times 0.03$ and three longitudinal segments. The slow readout channels would be brought out through various gas ports located along the top of the vessel resulting in a cable length of ≈ 12 m.

For the hadronic calorimeter, it was assumed that transformer matching would be employed and the requirement that the preamplifiers be located outside the magnetic field results in a maximum cable length of ≈ 6 m (again assuming that one penetrates directly through the cryostat). For the purpose of the study of electronic noise and pileup, it was assumed that there was only 1 longitudinal segment in the precision calorimeter thus resulting in 8700 such channels.

In spite of the 200 - 400 nsec drift time and the minimum rise time dictated by the cable length, the use of fast pulse shaping (qualitatively, differentiation) can result in the formation of a rather fast signal (with a corresponding loss in the charge sampled). Needless to say, there is also a corresponding increase in the equivalent noise charge (ENC). The optimal shaping time will be determined by a balance between the ENC, which increases as the shaping time is decreased, and the effective RMS noise due to pileup, which decreases as the shaping time is decreased.

The expected electronic noise for the three types of readout, fast electromagnetic, slow electromagnetic, and (fast) hadronic, was evaluated with reasonable care both from an absolute point of view and by scaling the measured results of NA34; the details are presented in the Electronics Group report[17] and the results are summarized in Table 2.

Quantity	Symbol	EM Slow	EM Fast	Hadronic
Pad Capacitance	C_{pad}	0.25 nF	2.8 nF	51 nF
Stripline Capacitance	C_{strip}	0.28 nF	0.8 nF	
Cable Capacitance	C_{cable}	0.90 nF	1.8 nF	9 nF
Total Capacitance	C_{source}	1.4 nF	5.4 nF	60 nF
Risetime	t_r	325 nsec	65 nsec	365 nsec
Measurement or Peaking time	t_m	400 nsec	100 nsec	500 nsec
Equivalent Noise Charge	ENC	4800 e	25000 e	30000 e
Equivalent Noise Energy	ENE	15 MeV	65 MeV	120 MeV
Uranium Noise Energy	σ_{ur}	5 MeV	7 MeV	170 MeV
Event Pileup Noise		115 MeV	120 MeV	113 MeV
Time Resolution (E = 5 GeV)		4 nsec	2 nsec	8 nsec

Table 2
Summary of Capacitance, Equivalent Noise Charge, Equivalent Noise Energy, Risetime, Event Pileup, and Time Resolution for the Calorimeter System.

The effects of event pileup are of fundamental importance and considerable effort was dedicated to its evaluation. Yamashita and Kondo[17a] calculated the RMS noise using events generated by ISAJET and assuming bipolar shaping. They included energy sharing, both transverse and longitudinal, among the towers. Alverson and Huston performed a similar calculation, which did not attempt to evaluate energy sharing, but which did verify explicitly the scaling of the noise with time and size of the tower. The estimated noise, scaled to the same parameters as were assumed for the electronic noise, is presented in Table 2.[17]

Missing E_t

The discovery of a number of new phenomena may rely heavily on the detection of missing neutrinos, or other weakly interacting particles, as evidenced by the observation of a large missing transverse momentum. The Calorimeter and Jets and Missing E_t groups made significant progress in studying a variety of effects which can simulate missing momentum.

A fundamental background is of course the extent to which known physical processes produce neutrinos. The level of neutrino production in jets, as characterized both by the mean multiplicity of neutrinos and the fraction of the initial parton momentum taken off by neutrinos, was studied by Iwasaki[18]. Results on the latter are presented in Figure 5 for light quarks, c, b, and t, quarks, and gluons with an inital momentum of 1 TeV. It is apparent that events with a t quark of large transverse momentum will often have a significant missing p_t. While this signature will be useful in tagging such events, it may also be a background to other, more exotic new processes.

It has been known for some time that events in which jets exit the detector through the beam pipe can yield a large missing momentum. The study performed at this workshop[18], using the latest version of Isajet in which initial gluon radiation is included, indicated that this effect is substantially worse than had been previously thought. The results are presented in Figure 6. The apparent missing p_t due to this effect will dominate the rate of events with real missing neutrinos for p_t up to nearly 100 GeV even if the calorimeter coverage extends to angles as small as 0.5 degrees. Fortunately given a distance of the forward calorimeter of 17 m from the crossing point, it should be possible to tag the existence of large amounts of energy at angles significantly less than 0.5 degrees, even if that energy cannot be precisely measured due to inadequate containment in the calorimeter.

The effects of multiple event pileup on missing p_t were also investigated. Figure 7 illustrates the distribution of missing p_t in the absence of any pileup, and with pileup for the case of bipolar shaping of duration 400nsec, as calculated by Alverson and Huson[19]. The pileup effects can be reduced by cuts on the sign and magnitude of the energy distributions in each tower.

It is quite possible that each of the above effects-loss of energy through the beam pipe and noise from pileup-will be small compared to the effects of cracks and dead spaces if the calorimeter is not properly designed. The large regions of non-uniform response implied by Figures 3 and 4 are rather disconcerting and it is important that detailed studies be performed to determine whether they present a serious problem or not. The use of warm ionization calorimeters, even if only for the electromagnetic section, would greatly alleviate the problem and the development of such calorimeters, such as is being carried out by UA1, is extremely important.

TRACKING

The tracking group reaffirmed once more the importance of quality tracking in order to accomplish the physics goals[20]. The specific motivations include:

1. Identification of electrons

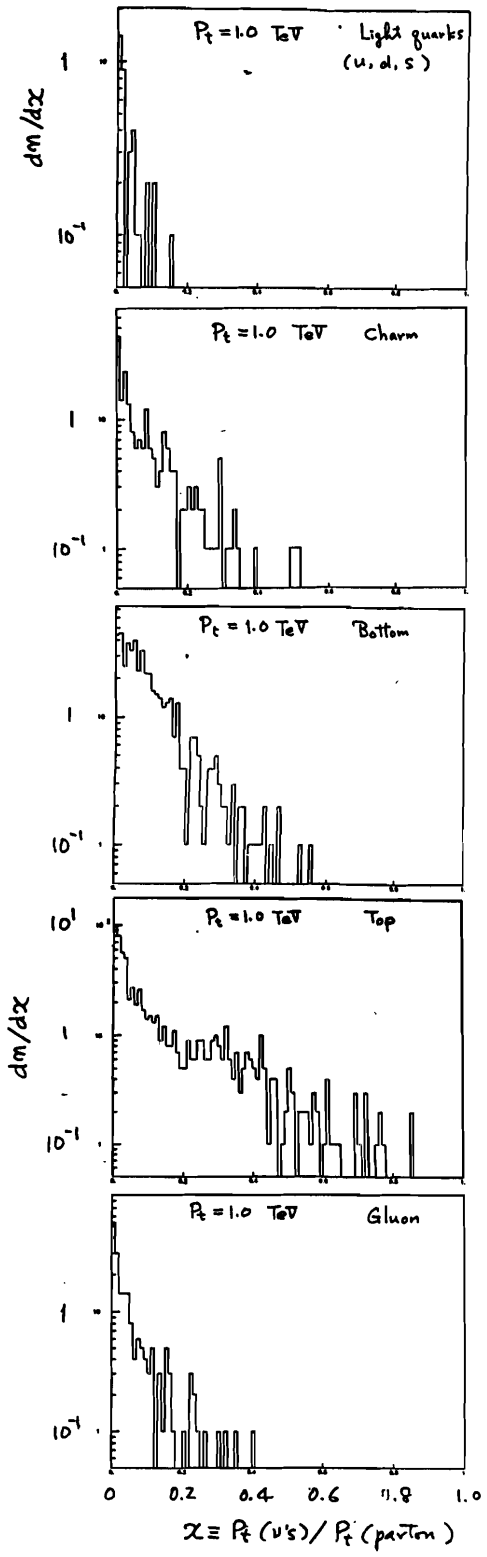

Figure 5
Distributions of the fraction, X, of the initial parton transverse momentum (1 TeV) that is carried off by neutrinos

2. Determination of whether there exists more than one interaction during a single crossing.

3. Matching of important signatures, such as electrons, muons, and high p_t jets with a particular vertex.

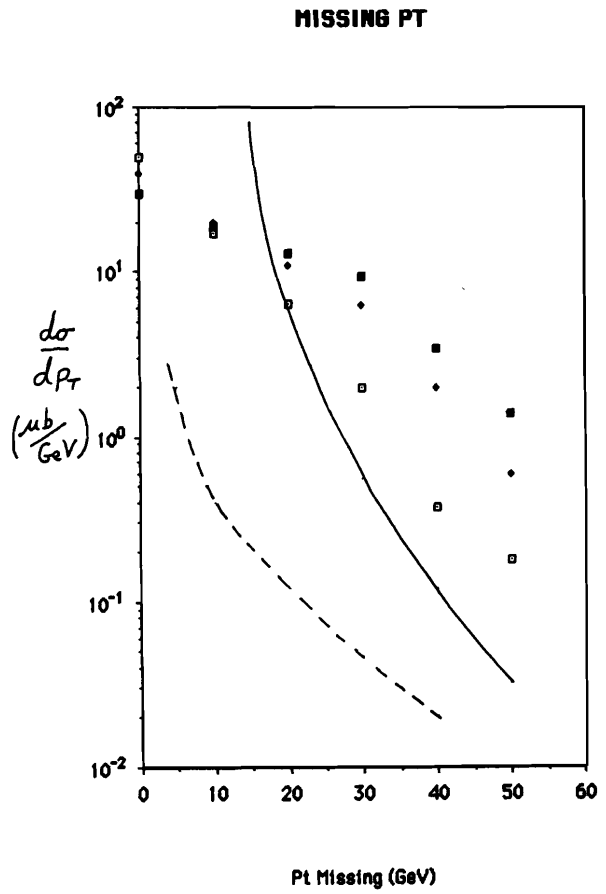

Figure 6
Missing p_t (Isajet 5.22) requiring $30 < p_t < 100$ GeV: solid squares below 2°, solid diamonds below 1° and open squares below 0.5°. The solid line is the missing p_t below 1.5° calculated at Snowmass '84 (Isajet 4.0). The dashed line is missing p_t contribution from neutrinos.

4. Identification and measurement of secondary vertices

5. Identification of τ particles

6. Improvement of missing E_t resolution by identification of high p_t tracks pointed to cracks or areas of poor resolution in the calorimeter.

7. improvement of e/π separation by comparison of momentum of track with energy observed in calorimeter.

8. Determination of the sign of electron

It should be noted that (4) - (8) require the presence of a magnetic field: for these reasons, and also on the general grounds that one should have the maximum capability to identify the unexpected, the consensus was that it is desirable to have a magnetic field. A solenoidal field geometry was studied, primarily because this geometry has been chosen by the bulk of colliding beam experiments, and because of the extreme importance of simple triggers. The relative merits of a dipole field versus a solenoid is certainly a topic worthy of further study.

Conventional Wire Chambers

Design Considerations Given the choice of a solenoidal

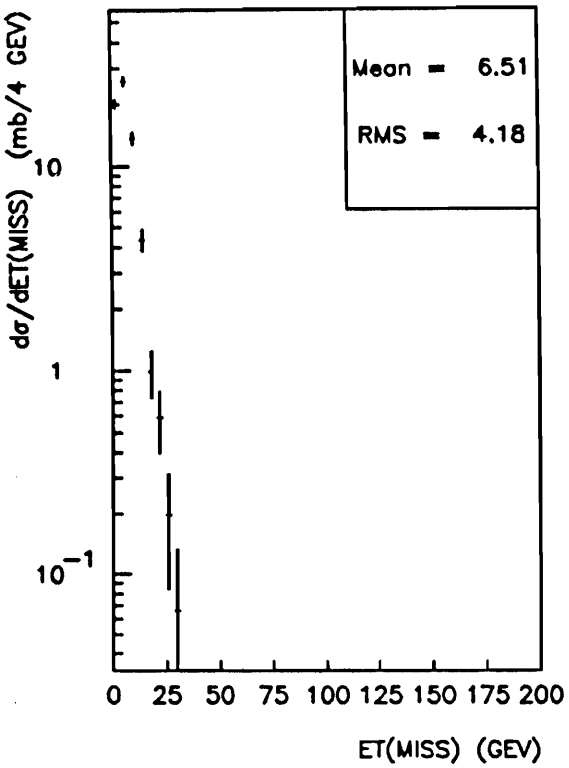

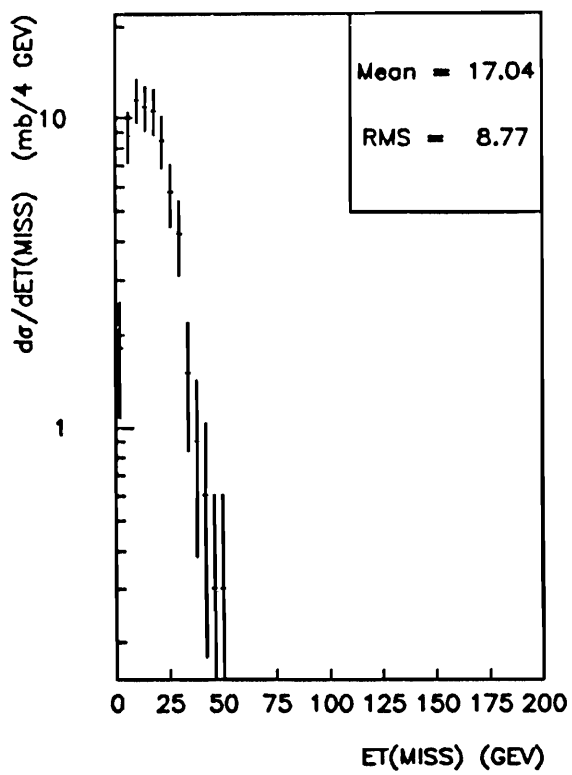

Figure 7
$d\sigma/dE_T^{miss}$ *(a)* In the absence of pileup. *(b)* Including the effects of pileup and assuming bipolar shaping of full width 400 nsec.

geometry, the bulk of the tracking detector in the central region will employ axial wires, and the primary design questions are (1) what is the optimal electrode configuration, (2) what is the best means of supporting the wires mechanically, and (3) what technique can one use to obtain the z coordinate. At angles less than 15 - 30°, one might well choose non-axial wires; this type of track detector was not discussed in detail, though its existence is illustrated in Figure 8.

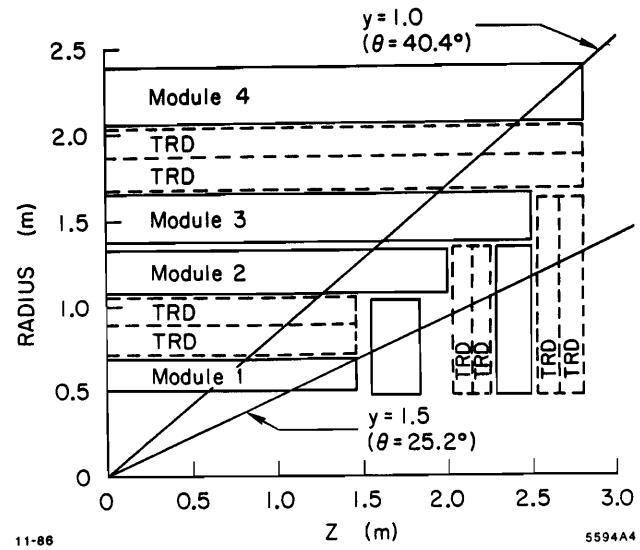

Figure 8
Schematic layout of track chambers in the central region ($|y| < 2$).

The electrode geometry and scale (cell size and total number of wires) are dictated by the simultaneous requirements set by considerations of radiation damage, rate limitations, and occupancy. The first must be satisfied if the chamber is to continue working for at least several years, the second by the requirement that the electric field not be distorted to the extent that drift times are incorrectly measured, and the third by the goal that track reconstruction efficiency be sufficient to accomplish the physics goals.

The onset of radiation damage in a chamber, the result of which is generally decreased gain and instability against H. V. breakdown, is usually parametrized in terms of the total collected charge per cm of wire length. In very clean laboratory environments, chambers have been operated, with little evidence of degradation, after charge collections in excess of 1 C/cm[21]. However, large chamber systems used in actual experiments often begin to deteriorate after charge collections 10 - 100 times less. For the purpose of designing for the SSC, it seems reasonable to assume that one will benefit from a better understanding of which gases to use and what impurities to particularly avoid; at the same time, some conservatism is called for in a very large and expensive system. We assume a goal of < 0.1 C/cm. Assuming an ionization of 100 electrons per cm, 10^8 interactions per second, and a gas gain of 2×10^4, a cell of 5 mm full width (and 1:1 aspect ratio) at $r = 25$ cm will accumulate 0.086 C/cm per year ($10^7 sec$). The same cell at $r = 50$ cm, would accumulate 0.11 C/cm in five years.

Changes in the gain and efficiency of wire chambers have been observed when the instantaneous rates exceed 10^4 particles per second per mm of wire length, for a gas gain $\approx 4 \times 10^5$. At lower gas gains, rates as high as 10^5 /mm-sec have been

obtained (in small chambers) without sigificant degradation[22]. A cell of 5 mm width at r = 50 cm experiences a counting rate of $\approx 2 \times 10^3$/mm-sec. An alternate criteria often used (though in principle less accurate) is the total current drawn per wire; typically, existing chambers begin to experience stability problems when this exceeds 1 uA per wire. Our canonical cell at 50 cm, if it covers $y < 1.5$ should experience a total current of $\approx$ 0.25 uA per wire.

The most stringent criterion for the cell size is in fact the average occupancy and the double track separation required to at least identify tracks of particular interest in the very high multiplicity environment typical of high p_t interactions at the SSC. A 5 mm wide cell (2.5 mm drift) has a resolving time of 50 nsec if a gas with conventional drift velocity (50 microns/nsec) is utilized. A layer of such cells at a radius of 25 cm and covering $y < 1.5$ would experience an occupancy of 28%, far above the range desired for useful tracking information. At r = 50 cm, the occupancy drops to a much more reasonable, but hardly conservative, 7%.

In order to provide tracking with conventional wire cells for radii less than 50 cm it will be necessary to utilize cells with a maximum drift of only 1-1.5 mm or a faster gas, or both. It is possible to obtain velocities of 100-125 microns/nsec with CF_4 which would help a great deal at small radii[24]. However, the lifetime of chambers operating with CF4 has not yet been adequately investigated.

To summarize, the considerations of radiation damage, instantaneous rate, and occupancy all dictate a cell size of the same order. The occupancy, which should be kept < 10%, is the most stringent requirement and implies cell sizes of order 2.5 mm, 5 mm and 9 mm for radii of 25 cm, 50 cm, and 200 cm respectively. Identification of a fast gas such as CF_4 which was sufficiently radiation resistant would improve the average occupancy significantly.

Cell Size and Shape With the small cell sizes discussed above, jet-cell geometries, which have been widely utilized at lower interaction rate machines, do not make much sense. (Figure 9) It is therefore assumed that individual cells, with an aspect ratio of roughly 1:1 will be used. These could be constructed with a number of different geometries, including square, hexagonal, or round (in the case of straws). In cells of this aspect ratio, there is little point to using multihit electronics. The effective double track resolution of a single cell is then just its half width. To obtain good efficiency for tracks spaced closely together, and to identify the time of any individual track, it will be desirable to stagger the cells in subsequent layers. To enable one to search locally in the chamber for segments, and to simplify the task of identifying the time of a segment, it may be beneficial to group the cells into superlayers of 6 layers each. There is considerable optimism that hardware processors, perhaps located directly on the chamber, may be able to reconstruct these segments sufficiently reliably that it will not be necessary to keep all of the raw hit information.

z coordinate Determination of the z coordinate will be particularly problematic. Charge division, which yields resolutions of $\sigma/l \approx 1\%$ for gas gains exceeding 10^5, is a poor candidate for gas gains on the order of $2 \quad 10^4$. It is likely therefore that one will have to rely on stereo measurements, supplemented by pad readout on a number of layers. The latter technique should yield resolutions of $\approx$ 1 - 2 mm on larger chambers, with much better accuracies obtainable on small chambers near the vertex. It was suggested that the axial and stereo wires might be grouped in an A U A V A arrangement where A and U,V represent the axial and stereo superlayers, each consisting of six wire layers.

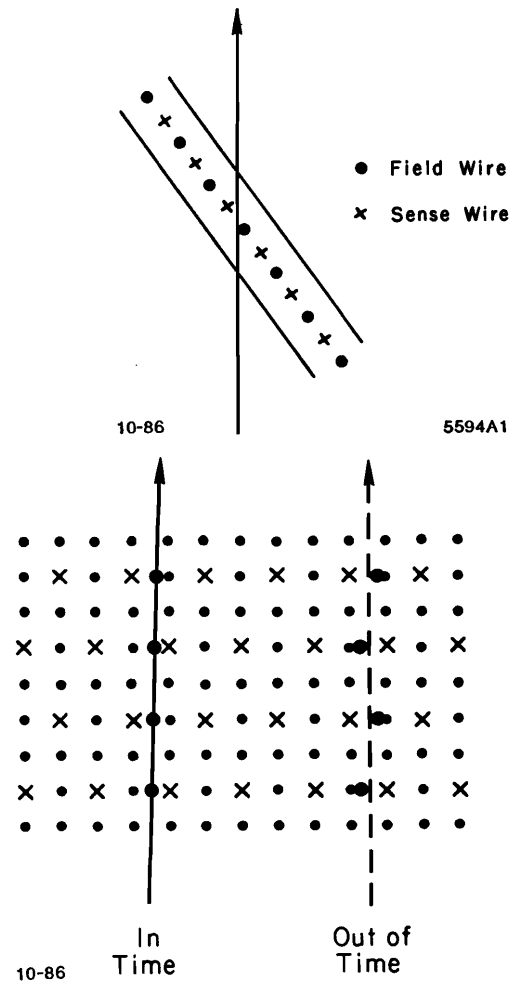

Figure 9
(Top) Conventional "jet cell" with maximum drift distance of a few mm. (Bottom) A possible small cell configuration; hexgonal cells could also be used. Hits from tracks that are out of time will not lie on a common trajectory.

Resolution and Number of Layers If the arguments concerning the cell size and shape are quite general and straightforward, conclusions concerning the required resolution and number of layers depend very strongly on the particular physics goals. One of the goals that was at least tentatively adopted is that one should be able to determine the sign of electrons for transverse momentum up to 1 TeV. This is obtainable with a resolution of 200 microns, 100 layers, and a field strength of 1.5 Tesla. Clearly this particular goal could be more economically achieved with half as many layers and an improved position resolution. It should be possible to obtain close to 100 microns in a reasonably straightforward fashion; alignment will be difficult but the excellent results achieved for L3 demonstrate that it should be feasible. Some suggest that by means of pressurized straws, it should be possible to obtain 50 micron resolution[24]. Such results have been obtained with straws, but to date only in much smaller devices.

The required number of layers will surely be determined primarily by questions of pattern recognition, and the trend of most experiments at lower energies to utilize of order 100 layers suggests it is unlikely that one will be able to do with less at SSC. However, a more quantitative answer to this question relies on considerable simulation, combined with a clearer

understanding of exactly what the tracking should be able to accomplish.

Mechanical Construction Assuming the cell sizes suggested above and the existence of 120 layers of wires, one estimates $\approx 1.3 \times 10^5$ sense wires. Since the wire tension for this number of wires is of order 80 - 100 tons, problems of supporting the wires are greatly alleviated if the chambers were built in 4 - 5 modules, as shown in Figure 8. In this case, one has only to support of order 20 tons per unit, and an endplate of thickness 1 cm may be used (with a safety factor of 8) A summary of the parameters of the chamber of conventional small cell construction is given in Table 3.

Module Number	1	2	3	4	Total
Drift Distance (cm)	0.20	0.35	0.40	0.50	
r_{min} (cm)	50	106	135	202	
r_{max} (cm)	66	130	162	235	
Number of Layers	30	30	30	30	120
Sense Wires	27,360	31,680	35,040	43,200	137,280
Average # Wires/Layer	912	1056	1168	1440	
Maximum Q (C/cm/yr)	0.019	0.007	0.005	0.003	
$\lvert y_{max} \rvert$	1.5	1.2	1.2	1.0	
Length (cm)	279	392	489	553	
Maximum Occupancy	0.094	0.105	0.106	0.091	
Maximum Current (μA)	0.528	0.288	0.253	0.194	

Table 3
Summary of Drift Chamber Geometry, Current and Occupancy

An alternative mode of construction might be to build each of the chamber modules entirely out of straws[24]. Straws offer a number of advantages including the absence of field wires which implies greatly reduced tension and thin endplates, isolation of broken wires, longer chamber lifetime, and the greater ease with which wires can be supported over long distances. On the other hand, the only such chambers built to date utilize straws which have a relatively large diameter (5 - 7 mm) and which are relatively short (70 - 100 cm).

The limits on wire stability[25] are similar for both types of chamber. For example, for wires one obtains limits of $l < 1.7m$ for 2 mm drift and $l < 4$ m for 5 mm drift; for straws, one obtains $l < 1.8$ m for 2 mm drift and $l < 5$ m for 5 mm drift.

For the conventional wire chamber, it was suggested that the barrel supporting the endplates could be constructed from a sandwich of 1 mm Al, 1 cm Hexcell, and 1 mm Al. This, combined with the gas and the wires, results in $\approx 4.5\%$ of a radiation length per module. The straw construction resulted in a nearly identical thickness.

TRD and Electron Identification

The use of TRD's, as recommended by the electron group, could be incorporated if a modular chamber design were utilized. However, the total thickness of material, which then approaches 30% for the complete system, is such that the track multiplicity, at least in the outer portions of the chamber, would be increased by nearly 50%. Said another way, 20-25% of all tracks would not come from the primary vertex. These effects may be large enough that they would significantly compromise pattern recognition and electron identification. This question clearly needs to be evaluated in more detail.

Microvertex Detectors

Detection of secondary vertices is apt to be important at the SSC, both to aid in identifying heavy quarks such as b and c, and also as a general aid in searching for new physics. Thus a silicon vertex detector is considered an important part of a 4 π detector, even if at the present time potential radiation damage would appear to limit its usage to luminosities less than 10^{33}.

The detector proposed is reasonably ambitious but not altogether implausible (Figure 10). Consisting of five layers of silicon at radii ranging from 5 cm to 15 cm, it would be constructed from 488 wafers, approximately twice the number being considered for the CDF silicon detector. The suggested strip pitch is 25 microns on the first three layers and 50 microns on the latter two layers, thus resulting in a total of 920k channels.

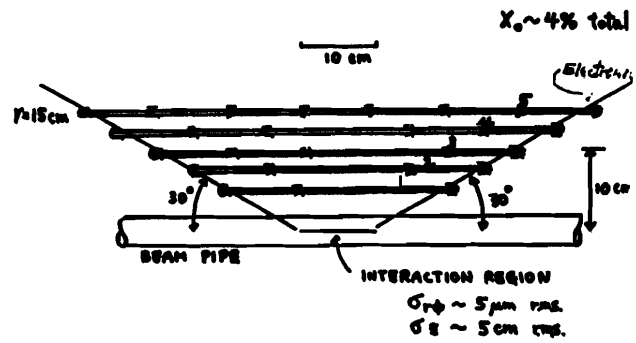

Figure 10
Schematic diagram of a five layer silicon microvertex detector. Two planes are used in each layer to determine r, ϕ and z.

The present developments of CMOS charge preamplifiers indicate that it may be possible to attain sufficient signal-to-noise if shaping times of several hundred nanoseconds are utilized. While this is long compared to the crossing time, it is estimated that the hit rate per strip is only 64 kHz even on the innermost layer. It may therefore be possible to operate the device with shaping times this long if analog buffers are incorporated along with the preamplifier and if the time of the hits is determined as well as the charge.

The power dissipation, even using CMOS biased at currents of one hundred microamps will pose a non-trivial problem for this number of channels.

There is currently a lot of enthusiasm for the development of true pixel detectors as a solution to the problem of secondary vertex detection at the SSC. It is too early to tell whether realistic devices can be built but it is certainly an important area of development.

Can one in fact identify secondary vertices in the extremely dense tracking environment of typical SSC events? Events were generated in which $b\bar{b}$ pairs were generated with transverse momenta of 500 GeV/c and the charged particles were tracked through a magnetic field of 1.5 Tesla. A glance at Figure 11a would seem to offer little hope that secondary vertices could be isolated. However, when the event is viewed on a very blown up scale (Figure 11b), appropriate to the resolution and double track separation of the vertex detector, it appears that it should be possible to identify the vertices in at least a reasonable fraction of the events.

ELECTRON IDENTIFICATION

The report of the group studying electron identification concentrated on four different topics[9]. These are:

1. The *requirements* for electron identification. For a variety of interesting physics topics, an attempt was made to de-

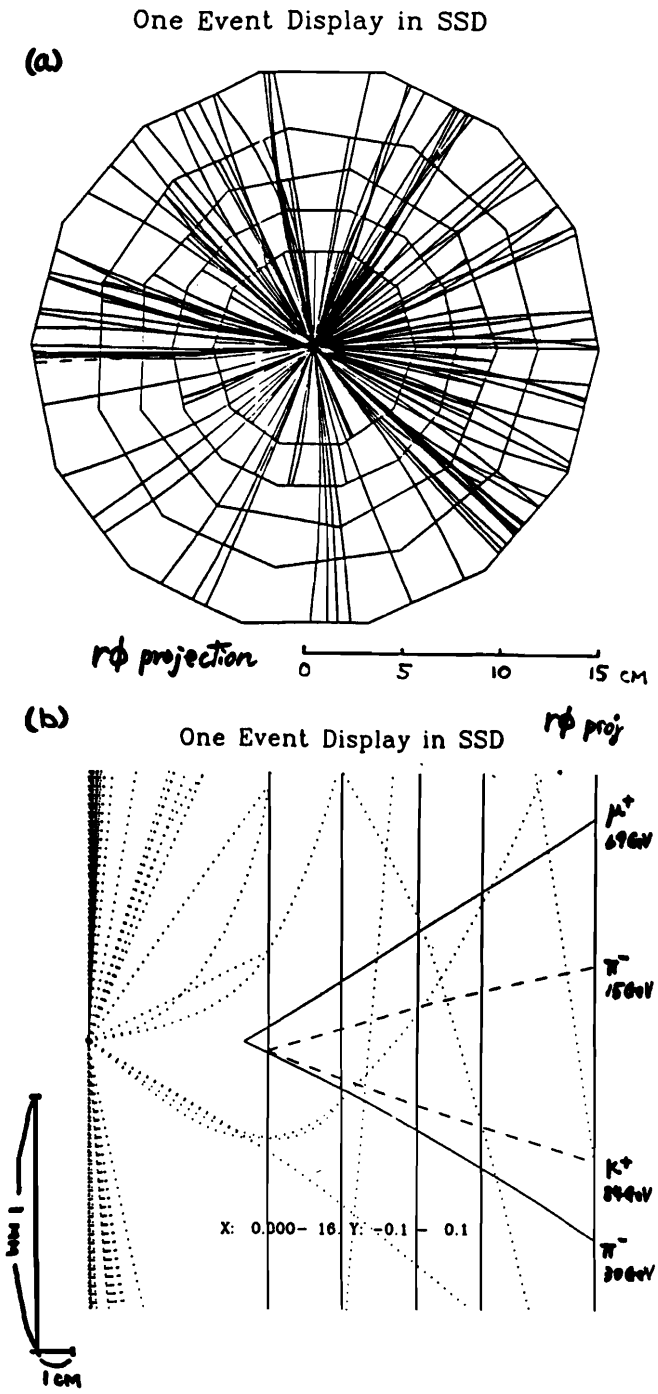

Figure 11
(a) Event display for a pair of $b\bar{b}$ jets, each with transverse momentum of 500 GeV/c. (b) The same event shown on a greatly expanded scale. The secondary vertex results from the decay of a B meson with 344 GeV/c p_t.

termine the rejection against hadrons that is required in order to identify or measure a particular physics process.

2. *Techniques* of electron identification. Special consideration was given to calorimetry, transition radiation detection (TRD), and synchrotron radiation.

3. *Backgrounds.* These include primarily the interaction of single hadrons, photon conversions, and the overlap of a charged particle with one or more photons.

4. *Overall detector design.* To what extent are the requirements for electron identification consistent with other goals for the overall detector.

We shall summarize each of these in turn.

Requirements for Electron Identification

Numerous studies have been made in previous workshops[7], as well as in the present one, on the topic of electron identification and its importance for the selection of physics processes of particular interest. It has already been noted in the section on calorimetry that studies of the identification of t-quarks at high p_t indicate that a calorimeter segmentation of order $\Delta\eta \times \Delta\phi \approx 0.02 \times 0.02 - 0.03 \times 0.03$ is required if one is to identify electrons efficiently. A study by Lane and Rohlf[26], also on the selection of $t\bar{t}$ events, concluded that such events could be selected cleanly if the rejection against hadrons simulating electrons exceeded a few $\times 10^3$. Since one is interested in searching for new particles, which might decay to $t\bar{t}$, in the mass range 0.2 - 1.0 TeV and since the lepton will carry off on average one third of the momentum of the parent quark the scale of interesting lepton momenta for this process is 20 - 150 GeV.

A process which is indicative of the electron identification required at very high energies is the production of a heavy Z' or W'. A study of this process[27] indicated that a W' or Z' with a mass of 1 TeV could be cleanly identified if a hadron rejection of order 10^3 can be obtained for leptons with transverse momenta up to 500 GeV/c.

In spite of the very high energy of the SSC, there will be a desire to identify leptons at rather low transverse momentum. As has already been metioned, the study of particles which decay to t quarks benefits from lepton identification down to transverse momentum of 20 - 30 GeV/c. The selection of b quarks, which may still be important at the time of the SSC for studies of rare b decays and CP violation, will benefit from lepton identification down to transverse momenta of *several GeV* since the b quark itself is produced most often at low transverse momenta. For studies of these processes, a rejection against hadrons of $10^3 - 10^4$ will be desired.

All of the studies that have been performed on the pion - electron rejection ratio that is required for selection of particular physics processes are inherently somewhat fuzzy in their conclusions, due to uncertainties in the backgrounds. The qualitative conclusion reached by the electron group during Snowmass 86 was that below 100 GeV/c many physics signatures would benefit from hadron rejection approaching 10^5 while for the regime above 1 TeV/c, rejections at the level of 10^3 would suffice.

One should perhaps also be guided by the experience of many generations of experiments at fixed target machines and at the ISR. The inclusive lepton-to-pion ratio is of order 10^{-4} roughly independent of p_t, except at the very lowest transverse momenta. Since the ratio of b-quark to light quark production in jets will likely be of order $10^{-2} - 10^{-3}$ and since the b-quark leptonic branching ratio is ≈ 0.1, the lepton/pion ratio is likely to be of order $10^{-3} - 10^{-4}$ at larger momenta as well. Thus, if interesting events are to be selected primarily on the basis of the lepton signature, rejections approaching 10^4 will be required. Where multiple selection criteria are employed, weaker rejections may be sufficient.

Electron Detection Methods

Calorimetry Many previous studies[28] have been performed on the degree to which one can distinguish electrons and hadrons using the longitudinal and transverse energy depositions in finely segmented calorimeters; it has been clearly established that high energy electrons can be distinguised from hadrons with rejection factors approaching 1000:1. It should be noted, however, that these results are invariably obtained in an environment where the particle under consideration was well separated from any other particles. In addition, the *optimal* transverse and longitudinal segmentation, given the invariable limitations of cost and complexity, is not so easily stated, particularly when it is desired to identify electrons over a very wide range of energies.

Two general questions addressed by the electron group at this workshop were (1) the optimization of the calorimeter parameters for the best electron identification and (2) improvements in the methodology of electron selection in order to find faster and more efficient algorithms. Each of these topics benefited from a study by Y. Fukui[29] of electron identification, and hadron rejection, using test beam data in the End Plug calorimeter of CDF. This calorimeter utilizes a tower readout ($\Delta\eta \times \Delta\phi \approx 0.1 \times 0.1$) for the first 2.5 and last 2.5 radiation lengths, and a combination of strip and tower readout for the central twelve radiation lengths. The strips are alternately oriented to measure accurately the width of the shower in η or ϕ. The three longitudinal tower readouts are referred to in Figure 12 as EM1, EM2, and EM3 while the strip readout is referred to simply as η or ϕ. A six interaction length hadron calorimeter was also used; its readout will be designated as HAD.

The technique for the analysis is to calculate a χ^2 variable for an individual event to evaluate the probability that the observed energy distributions are consistent with those expected for an electron. The method uses the full covariance matrix evaluated from electron test beam data and thus takes into account not only the average values of the measured variables $\{v_i\}$ but their correlations as well:

$$M_{ij} = \frac{1}{N}\sum_n (v_i^{(n)} - \bar{v}_i)(v_j^{(n)} - \bar{v}_j)$$

$$H = M^{-1}$$

$$\xi_m = \sum_{i,j} (v_i^{(m)} - \bar{v}_i) H_{ij} (v_j^{(m)} - \bar{v}_j)$$

The parameter ξ_m is a χ^2 measure of how well event m agrees with the mean values and correlations v_i appropriate to the calibration sample used to determine M. The reader is referred to the electron group report and to the specific study[9,29] for details of the analysis. Here we simply summarize the notable features and conclusions.

While the procedure is potentially very general and powerful, it can require a determination of M as a function of energy, position, and incident angle. One of the significant contributions of Fukui et al was to recognize that using ratios of the energy deposition in individual layers to the total deposition removes to first order the energy variation of the variables and hence of the matrix M. Secondly, by using energy weighted rms widths as a measure of transverse shower size one obtains a measure of the transverse size which is largely independent of the impact point.

Figure 12 shows the pion rejection factor as a function of electron efficiency for 100 GeV electrons and pions. For an electron efficiency of 90%, a simple comparison of the energy after $17X^o$ to the deposit in the first $17X^o$ gives a rejection of order 50. The additional rejection obtained by using longitudinal shower shape within the EM calorimeter is 2-5 and that obtained by using the transverse shower size is another factor of 2-3. The overall rejection factor of 400 for 100 GeV has not directly used the absolute energy deposit in the EM section. It is quite likely that further optimization of the algorithm and of the segmentation would lead to further improvements. We conclude simply by noting that this study, in addition to contributing some ideas concerning intelligent choice of variables for the general χ^2 approach, corroborates earlier measurements that rejections of order 1000:1 may be obtained.

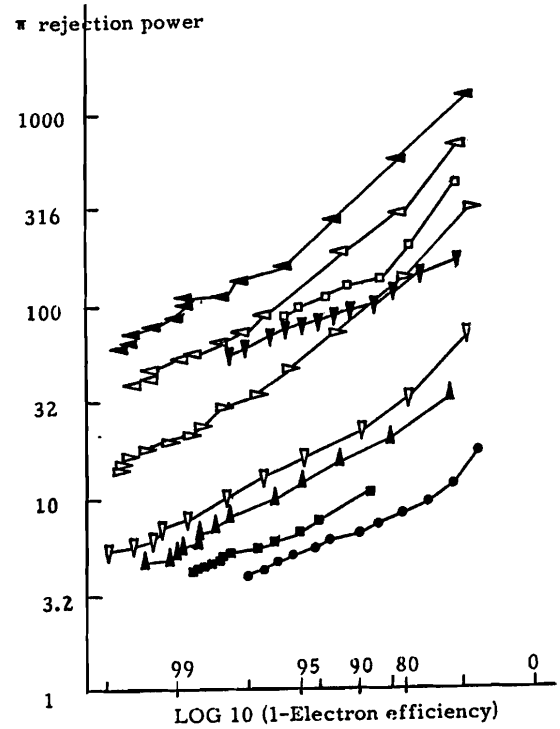

Figure 12

π rejection power as a function of electron efficiency for 100 GeV e^- and π^- events. The set of variables used is denoted by:

- EM1,EM2,EM3/EM $+\eta+\phi$ $+\sigma_\eta+\sigma_\phi$ +HAD/EM
- EM1,EM2,EM3/EM $+\eta+\phi$ +HAD/EM
- EM3,(EM1+EM2)/EM
- HAD/EM
- EM1,EM2,EM3/EM $+\eta+\phi$ $+\sigma_\eta+\sigma_\phi$
- EM1,EM2,EM3/EM $+\eta+\phi$
- EM1,EM2,EM3/EM
- EM3,(EM1+EM2)/EM
- EM1,(EM2+EM3)/EM

Transition Radiation Detectors Transition radiation detectors have been used for electron identification in several fixed target and colliding beam experiments, and will be included on a major scale in both the D0 detector[14] at Fermilab and the upgraded UA2 detector at CERN.[30] Their use in SSC detectors has has been discussed previously, but potential problems included (1) the relatively large amount of space required (40 - 50 cm per module), (2) the long collection time if drift distances of several cm are used, and (3) the fact that in previous geometries considered the upper limit for efficient electron discrimination was $\approx$ 100 GeV/c. A design was developed at this workshop which appears (subject to some caveats) to overcome most of these problems.

Perhaps the most important observation is that one can "tune" the design of the radiator to improve the rejection of high energy pions. By utilizing polypropylene foils 40 microns thick and separated by 900 microns, one can increase the energy of the X-rays relative to earlier designs; Figure 13 shows the X-ray spectrum detected in a 4 cm Xenon chamber following a 100 foil radiator. In this way the effective threshold for pions can be increased to ≈ 300 GeV/c.

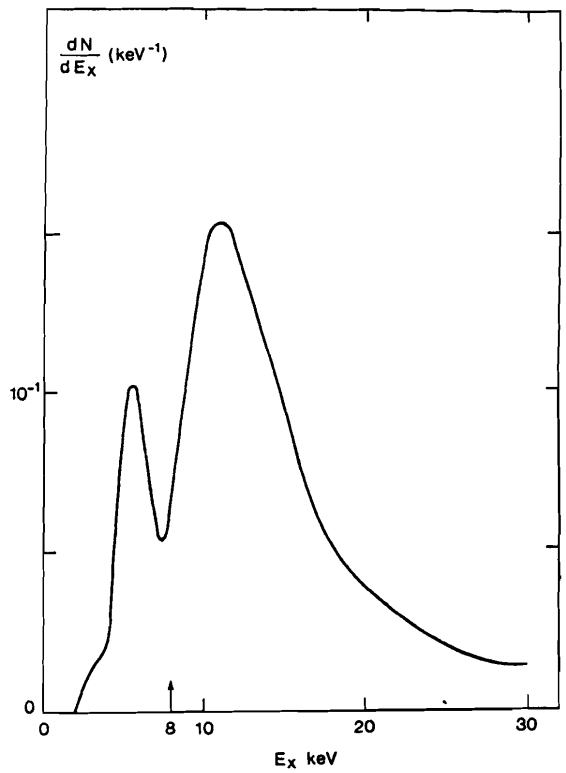

Figure 13
X-ray spectrum detected in each chamber.

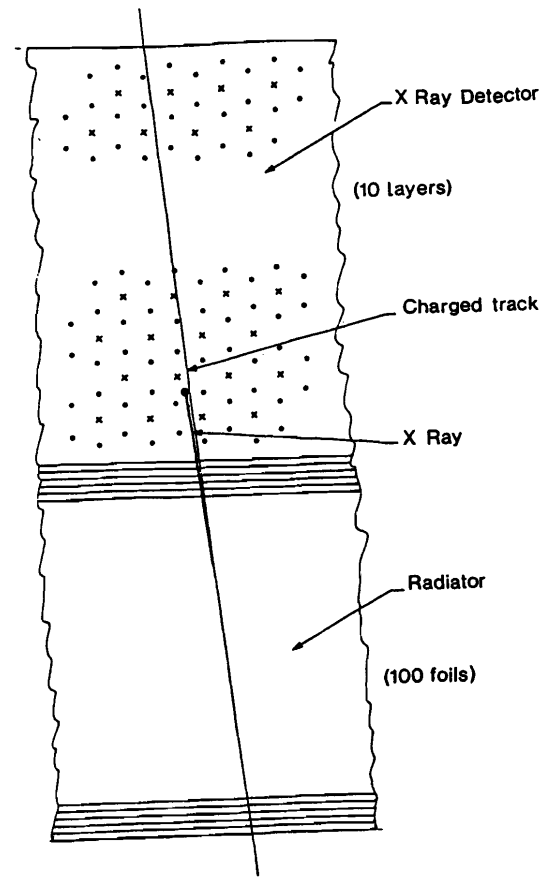

Figure 14
Schematic diagram of the TRD X-ray detector. Hexagonal cells are made of six potential wires and one sense wire and are 4 mm in diameter. The radiator consists of 100 foils of polypropylene 40 microns thick and separated by 900 microns.

To significantly decrease the collection time, it is suggested that the Xenon chamber following the radiator consist of 4 mm diameter hexagonal cells as shown in Figure 14. A prototype chamber very similar to this design has already been constructed by Bouclier et al[31] (though not necessarily for use with TRD's) using cells of only 2 mm diameter. If the chamber is filled with a mixture of $Xe - C_2H_6$ (50%-50%), the drift velocity is 45 microns/nsec for an electric field between 1300 and 2500 volts/cm: thus the time to collect all the charge is 45 nsec. The total thickness of the Xenon chamber would be approximately four centimeters.

For most particle trajectories (the exceptions being those occurring when the particle passes very near the sense wire) significant portions of the ionization energy loss drift nearly perpendicular to the track direction and will therefore arrive at the sense wire at approximately the same time; the technique of cluster counting may then not work as well as in a geometry where the drift field is always parallel to the track direction. Thus it was assumed that only the total charge in each cell would be measured.

The pion rejection factor was evaluated for a TRD system consisting of four radiator/chamber packages corresponding to a total thickness of 56 cm. It is apparent from Figure 13 that the ionization energy loss may be effectively discriminated against by requiring a minimum of 8 keV in any individual cell; the probability that a pion will yield more than 8 keV in a single cell is 2.1×10^{-3}. The electron-pion rejection for 50 GeV/c particles, obtained by selecting on the total charge of all those cells with greater than 8 keV each, is shown in Figure 15. One obtains a rejection of 34 for an electron efficiency of 90%. If instead one cuts on the number of cells which have charges exceeding the 8 keV cutoff, one obtains a rejection of 220. The same calculation for electrons and pions at 300 GeV/c yields a rejection of 5 using total charge and 15 using the number of cells above threshold. The Monte Carlo calculation yielding these results is somewhat idealized in that it does not take into account either the variation in path length in each hexagonal cell due to the position of the particle or charge sharing between neighboring cells.

If the electronics on each wire were designed to measure time as well as charge, then the position of energy depositions could also be determined, and each of the hexagonal cells could be considered a part of the tracking detector. It has already been pointed out in the section on tracking that there exists some motivation to group layers of the track detector together into superlayers, in order to allow the easy identification of track segments. If one further assumes an outer radius of the tracking of order 2 meters and a total of 100 measurements along a track, there will exist significant free space as a function of radius and one might argue that the TRD's can then be fully integrated with the tracking in a way that costs relatively little (other than the cost of the TRD itself). Whether this appealing integration of TRD's and the tracking system (which was already indicated in Figure 8) is really feasible or not will

depend in large measure on a more detailed examination of the details of the mechanical supports. In addition, it was already noted that the total amount of material is uncomfortably large.

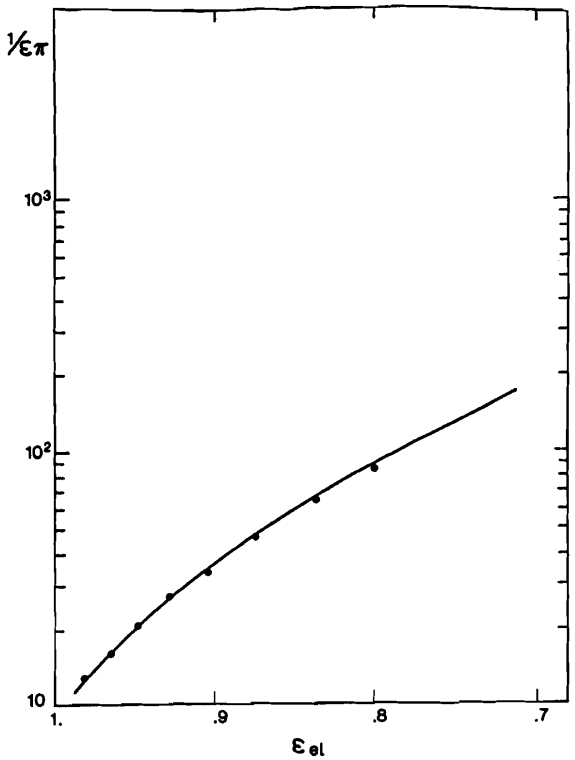

Figure 15
Pion rejection factor $(1/\epsilon_\pi)$ as a function of electron efficiency (ϵ_e) using total detected charge in four layers.

Synchrotron Radiation Synchrotron radiation has often been considered as an attractive possibility for electron identification and in fact is being used in the AMY detector at TRISTAN. Since the total radiated energy increases as E^4,

$$E_L(MeV) = 0.0885E^4(GeV)S/(2\pi R^2)$$

where S is the total path length in meters and R is the radius of curvature, one might expect this technique to be particularly fruitful at the high energies addressed at the SSC. One can rewrite the above expression as

$$E_L(MeV) = 1.26 \cdot 10^{-5} S E^2 B^2.$$

In addition, it may be shown that the *number of photons emitted* is only a function of B $\times$ S and is independent of energy. It is therefore the average energy of the photons that increases dramatically with the energy of the incident particle. For particles of several hundred GeV momentum, the majority of the photons emitted have energies exceeding the critical energy of many heavy Z materials. As an example, if $B \approx 15$ kG and $S \approx 1$ m, the number of photons of energy > 5 MeV is about 10 for electrons of energy 200 GeV.

Detection of these photons is not altogether simple because of their high energy. In the 5-10 MeV region the mass absorption coefficient in lead is about 0.45 cm, with about half the cross section due to the pair production process. Thus nearly 0.9 cm of lead will be required in order to yield 3-5 conversions thereby producing 6-10 electrons and positrons. The lead must be segmented into several thin sheets with active sampling material in between if these electrons and positrons of a few MeV are to be detected. The signature for a primary electron would then be a large signal in this several layer very fine sampling "calorimeter" while hadrons would yield the usual Landau energy loss distribution.

The reader has probably already noted that 0.9 cm of lead corresponds to 1.6 radiation lengths and that the primary electron will often produce much more dramatic effects when interacting with this much material. Indeed, the amount of lead suggested above and the nature of the signature is nearly identical to what is employed in the UA2 "preconverter". Thus in evaluating the merits of synchrotron radiation as a tool for identifying electrons, it appears important, particularly in the central region where the syncrotron radiation is only marginally separated from the track trajectory, to compare the anticipated signal with that produced by interaction of the primary electron in the synchrotron radiation detector.

Detection of synchrotron radiation may be most applicable in the forward region, for those detectors which include strong magnetic fields in that region. This follows for two reasons: first, much longer path lengths are typically available, thereby allowing the synchrotron radiation to separate more from the initial particle trajectory. Such a separation is a feature that is qualitatively different from the early showering of an electron (or hadron) and may therefore improve the selectivity of electron detection. Secondly, the momenta of electrons of even moderate p_t (e.g. 50 - 100 GeV/c) are very large thus rendering techniques such as TRD's of limited use.

Backgrounds

Consideration was also given to the dominant sources of background which can mimic an electron signature, those being single pion misidentification, photon conversions (plus Dalitz decays), and overlaps between a charged hadron and one or more photons. We give a very brief summary of these discussions.[9]

Pion Misidentification As noted earlier, it is to be expected that a well-designed calorimeter can achieve rejections of hadrons (at least in an isolated environment) of order 1000:1. In some cases, rejections even higher than this may be obtained; however, diffractive interaction of pions into final states in which most of the energy is taken off by neutral particles sets a fundamental limit at the level of $\approx$ 3000:1 on the rejection that can be obtained by a calorimeter alone. Transition radiation detectors should yield independent rejections of 50 - 100, however, and hence it should be possible with a combined system to obtain a total rejection near 10^5.

Conversion Backgrounds The rejection factor R that can be obtained against conversion pair backgrounds can be written

$$R = (dN_D/dN_p)P_c e_{pair} P_v$$

where the quantity in brackets is the parent- daughter relation for π^o decay, that is the ratio of the number of photons to π^o at a given energy, P_c is the total (internal plus external) conversion probability, e_{pair} is the efficiency for identifying the conversion as a pair of tracks, and P_v is the probability of identifying the conversion by the absence of a pointing track upstream of the conversion.

The parent-daughter relation depends strongly on the p_t distribution and for an exponential distribution is of order $< p_t / p_t$. However for a power-law distribution the ratio approaches a constant value at large p_t. For the p_t^{-5} factor expected from QCD, $(dN_D/dN_p) \approx 0.44$.

The photon conversion probability P_c is determined by the amount of material. For the track detector discussed above the

amount of material at 90° is nearly 20% of a radiation length, not including the additional material due to the TRD's. In addition, it is unlikely that the end plates of the chambers can be reduced to less than 20% even if great care is taken to reduce the material in the wire support and electronic systems.

Identification of the conversion by the detection of two, rather than one, charged particles may be achieved either by the use of dE/dx (in scintillator, silicon, or wire chambers) or by the direct observation of two tracks. For the former case, which is generally used in non-magnetic detectors, it is anticipated that a rejection of order 100 may be obtained with suitable measurements of dE/dx. The latter case is more complicated since it depends on tracking efficiency at low momentum; an estimate is given as a function of photon energy and the assumed minimum momentum at which tracks can be efficiently identified, in the Electron Group Report. At the risk of oversimplification, it seems reasonable to assume that rejections of 50 - 100 are feasible.

Finally, it was noted that the efficiency with which one can identify conversions by the absence of a pointing track will be limited by the track density in the event as a whole. It was estimated that, assuming an isolation equivalent to that required by the calorimeter segmentation, one would obtain $P_v \approx 10-20$.

It is apparent from the above that the overall efficiency for identifying conversions is a relatively complicated function of energy and angle; the conclusion is that it should be possible to achieve rejections approaching 5×10^4 10^5.

Overlap Backgrounds Finally we consider apparent electron signatures produced by the spatial overlap of a charged particle and one or more photons. One study using an EM calorimeter with fine depth segmentation and one-dimensional transverse segmentation found that exactly overlapped photons and pions, produced with energy spectra appropriate to high energy collisions, could be rejected at the level of 100:1[32]. A crude estimate of the overlap probability for a charged particle and a photon indicated that even taking particle densities appropriate to a 500 GeV jet, the probability that a given charged particle would be overlapped within 1 cm by a photon was less than 1%. One should also note that TRD's should reject this background with nearly the same efficiency as is obtained for single hadrons. While relatively large uncertainties clearly remain, it appears that rejections substantially in excess of 10^4 can also be obtained against this background.

MUON DETECTION

Introduction

The muon group considered in some detail a rather broad range of the issues relevant to muon detection including physics topics for which muon detection may be particularly important, the basic geometry of the detector, fundamental limitations due to catastrophic energy loss mechanisms, momentum resolution, and triggering.[33] We discuss each of these briefly in turn.

Importance for Physics

While few people would question the importance of a good system for muon identification and measurement, it is useful to restate briefly some of the reasons that muon identification may be particularly important.

1. *Sign of leptons* New Z's which decay to lepton pairs have characteristic asymmetries which may enable one to deduce the extended gauge group to which they belong. In addition, like-sign leptons are key signatures for Majorana neutrino pairs if suitable kinematic selections are made. It is important that the sign of leptons be measured in the forward direction, a region in which the sign of electrons may not be easily determined.

2. *Muons are more easily identified in jets* than electrons. Many physics topics may benefit significantly from identification of leptons in, or near, jets. Such identification will be very difficult for electrons.

3. *Muon-electron correlations* are important for determining whether events with multi-leptons are produced by (a) pairs via a neutral current, (b) uncorrelated weak decays of heavy quarks, or (c) exotic decay processes.

4. *Very Forward detection* may be easier for muons than for electrons. One of the leptons from a high-mass pair is often emitted at small angles.

5. Reasonable mass resolution may be obtained in combination with sign information. While the mass resolution of very high mass pairs will be superior for electron pairs, it may be difficult for such events to obtain a sign determination for both electrons.

Figure 16 illustrates the importance of acceptance down to fairly small angles, even for Z masses as large as 2 TeV.

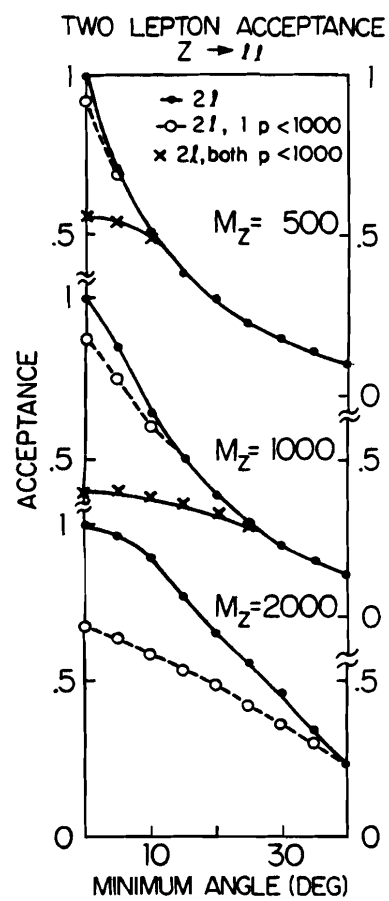

Figure 16
Two-lepton angular acceptance for $Z_\chi \to ll$ for Z masses of 500, 1000 and 2000 GeV.

Measurement of the sign asymmetry can be important both for determining the coupling of a new boson to u and d quarks and for deducing the type of gauge group to which a new boson belongs.

Muon Detector Geometry

The basic layout of the muon detector considered is shown in Figure 17. The field in the central region traverses a 3m thick rectangular box; the direction of the field could be either axial or azimuthal depending on whether the flux from the solenoid is returned through the muon spectrometer or the hadron calorimeter. The endcap detector is square in cross section, is four meters thick, and contains a toroidal field which is excited by coils in a conventional manner. In the forward direction, a cylindrical toroid, of approximately 5 m thickness completes the angular coverage. The geometry of the detector considered could be adapted with minor variations to either the Model A or B detectors.

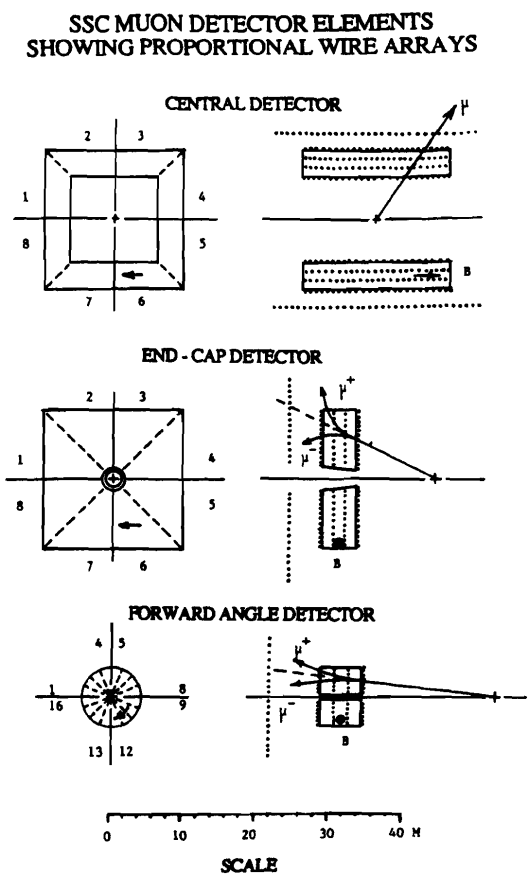

Figure 17
Magnetic and proportional wire detector geometry for the muon detector. A total of 108K electronic wire detector channels is needed.

Also illustrated in Figure 17 is the proposed layout of detector planes. Each system contains a minimum of five detector planes. This choice is motivated by the desirability, for accuracy of momentum resolution, of measuring at least the exit or entrance angle, as well as measuring the sagitta. In addition, due to occasional large electromagnetic showers which may obscure the muon track, an additional detector plane must be included. Five planes were deemed sufficient for the central and endcap regions, though addition of a sixth plane allows somewhat improved momentum resolution. In the forward direction, the higher average energy of muons and the probable necessity of reasonably sophisticated triggering in hardware processors, may require six planes.

Each detector plane is comprised of three layers of drift tubes; the redundancy is necessary both to allow for inefficiency in a given layer and also to provide resolution of the left-right ambiguity and a corresponding determination of the time of the track to an accuracy such that it can be identified with a particular beam crossing. It is estimated that the total muon system then contains 108k wires. Assuming that the non-bend coordinate is determined (with reduced resolution) by charge division, charge induction on pads, or a comparison of the time of the signal at each end of the wire, the total number of electronic channels will be of order 220k.

Effect of Catastrophic Energy Losses

Muons of energy greater than several hundred GeV are subject to large energy losses when they traverse high Z materials due to bremstrahlung, pair production, and nuclear interactions. The Muon Group therefore invested considerable effort in investigating the effect of these energy losses on muon detection and momentum measurement. Figure 18 shows the distribution of exit momenta of a 2 TeV muon beam after traversing 3 m of iron, as calculated with Van Ginneken's TRAMU muon transport code. The full width at half maximum is 0.7%. Ten percent of the muons lost more than 2.5% of their energy, and 1.5% lost more than 10% of their energy. These fluctuations are negligible compared with the 10 - 12% lower limit on the momentum resolution due to coulomb scattering. The occurence of very large fractional energy losses at a rate of a fraction of a percent could have significant impact on the probability of observing large missing E_t however. While it is likely that such catastrophic energy losses can be identified by anomalous hits in one or more of the detector planes, this effect has not yet been studied in detail.

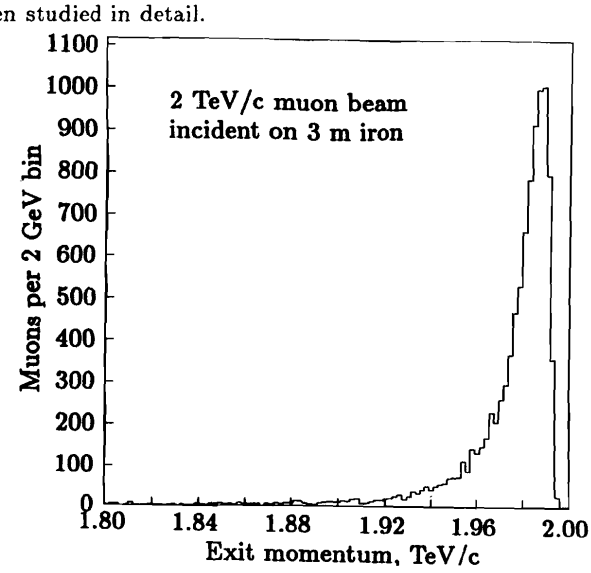

Figure 18
The momentum distribution of 2 TeV/c muons after traversing 3m of iron, as obtained with Van Ginneken's TRAMU muon transport code. The most probable loss is 13 GeV, and the full width at half maximum 14 GeV (0.7%). Ten percent lost more than 2.5% of their energy, and 1.5% lost more than 100% of their incident energy.

Of more direct importance for the detection of muons is the fact that showers of a few GeV, though they do not significantly change the energy of the muon, can obscure the muon track in one of the detector planes. This effect was evaluated with

some care. For example, if three chambers are utilized for a sagitta measurement and all three planes are required to be clean of additonal hits around the muon, it is estimated that the efficiency for a 1 Tev muon is only 60%; for a 3 Tev muon, the efficiency has fallen to 30%. It is necessary therefore to include at least one redundant plane. Fifty cm of iron between the detector planes was thought to be sufficient to eliminate correlations.

Momentum Resolution

The Muon group also considered in some detail a variety of schemes for momentum measurement. In comparing air core and iron core magnets they noted that since the fractional error due to coulomb scattering decreases as $L^{-0.5}$ while the fractional error due to measurement of the sagitta decreases at L^{2}, better resolution could in principle be obtained with air core magnets. An example is the muon spectrometer patterned after the L3 detector for which the momentum resolution was estimated to be $\approx 4\%$ at 1 TeV.[34] However, it was also concluded that iron core magnets would likely be used for the the general purpose 4π detectors because of the easier construction and the ability to combine the muon identification with the momentum measurement.

The measurement precision obtainable with an external iron muon spectrometer, of thickness 3 m and field strength 2 T, was evaluated for four different measurement strategies. In each case a basic set of three measurements, at the entrance of the iron, in the the center of the iron, and at the exit of the iron, was assumed. The four possibilities then supplemented this information with:

1. No additional measurements; i.e. one relies entirely on the sagitta measurement in the iron.

2. The muon direction at the entrance of the muon spectrometer is measured by providing an additional measurement with a lever arm of 1 m (assumed to be in iron, either with no magnetic field or a field perpendicular to the field in the external spectrometer).

3. Either the incoming or the outgoing angle of the track is measured assuming a 1 m lever arm in air.

4. The incoming direction is measured in iron, the outgoing in air; the optimum case (both directions in air) is not substantially different from this case.

These four different possibilities are schematically illustrated in Figure 19. In each case a position resolution (per superplane) of 100 microns was assumed. The results are compared in Table 4. It is apparent that for any substantial improvement one must measure both angles. Also shown in Table 4 are the results obtainable with the central track detector.

Momentum	(a)	(b)	(c)	(d)	(e)
200 GeV	12.4%	14.1%	12.3%	11.0%	4.6%
400 GeV	13.9%	15.2%	13.6%	11.7%	9.2%
700 GeV	17.3%	18.0%	16.6%	13.3%	16 %
1 TeV	21.7%	21.6%	20.4%	15.6%	23 %
2 TeV	38.2%	36.0%	35.3%	24.8%	46%

Table 4
Momentum resolution for four different measurement techniques in the muon spectrometer (refer to Figure 19) (a) iron only (b) 1 angle (in Fe) (c) 1 angle (in air) (d) 2 angles. For comparison the resolution obtainable with a central track chamber is also shown (e).

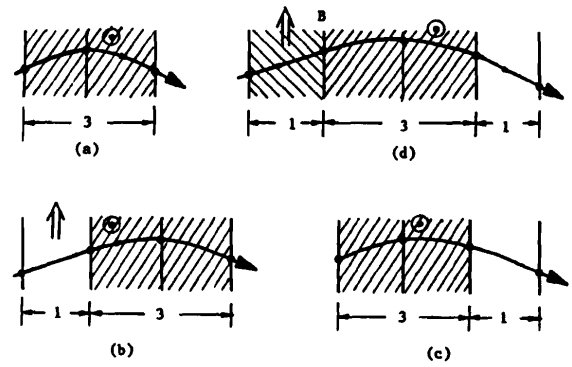

Figure 19
Muon momentum measurement schemes for various magnetized-iron geometries as described in the text.

A comparison of the resolution obtained with three superplanes of high precision (100 microns) plus angle measurement with one using the same 3 m of magnet, but divided into four superplanes with poorer position resolution, is shown in Figure 20. The latter assumes four planes in the iron, with 300 microns resolution, both with and without the initial angle measurement. It is apparent that the resolution is dramatically better if the higher resolution can be obtained; hence studies to understand whether one can achieve systematic errors approaching 100 microns for such a large spectrometer are very important.

Triggering

Considerable attention was devoted to the muon trigger, and this is discussed in the section on triggering below.

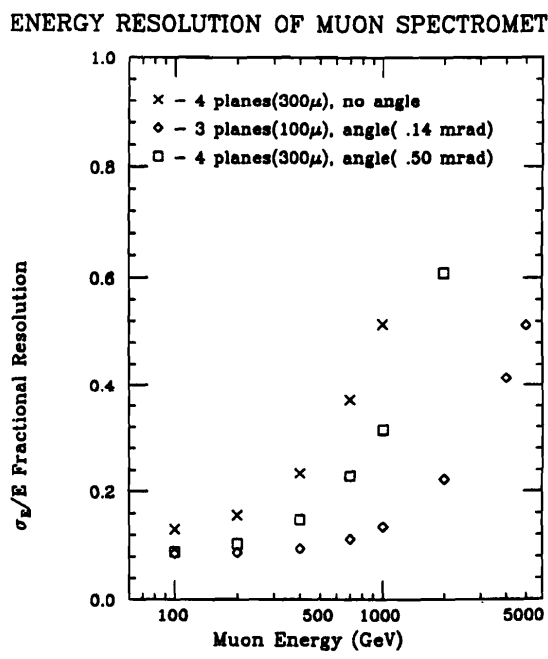

Figure 20
The resolution of the muon energy for various measurement strategies *i.e.* number of planes and the initial angle. (The resolution of the initial angle uses the point resolution in a plane for two planes separated by 1 m of air).

ELECTRONICS, TRIGGERING, AND DATA ACQUISITION

Introduction

It has already been noted in the discussions on calorimetry and tracking that a significant development of electronics will be required if experiments at the SSC are to adequately exploit the full luminosity available. This follows from the necessity of simultaneously satisfying the goals of high speed, low noise, and low power. The performance required, and the problems encountered, will be similar for many different types of experiments whether they utilize large 4π detectors, forward spectrometers, or other specialized detectors. The Electronics group concentrated on the systems required for large 4π detectors since it is for this application that many of the problems are most acute.[17]

A conceptual design for the overall system of electronics, triggering, and data acquisition is presented in Figure 21. The major considerations which lead to this design, which is a natural evolution of existing systems, include the following:

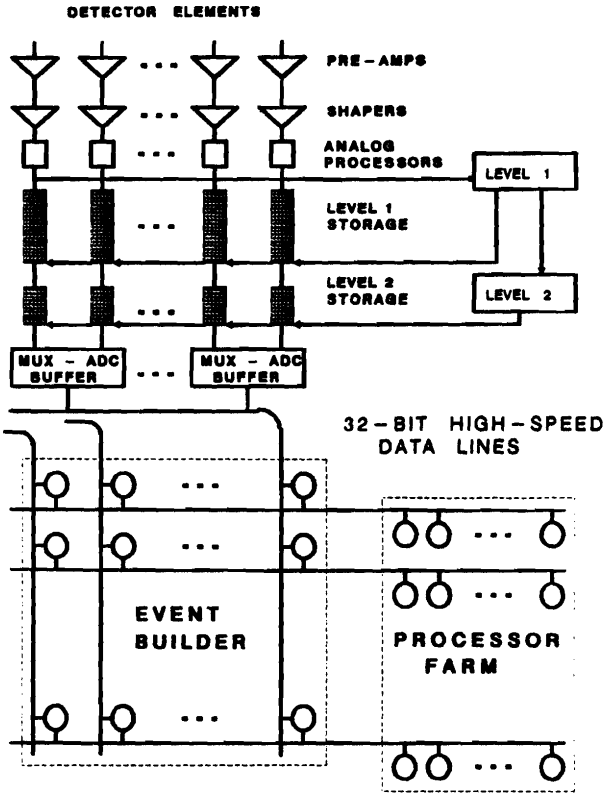

Figure 21
Schematic diagram showing the front end electronics, level 1 – level 2 buffers (primarily analog) multiplexer – ADC – digital buffer, event builder, and processor farm.

1. High luminosity, corresponding to an interaction rate of order 10^8 events per second, is essential if one is to be sensitive to many of the processes of greatest interest.

2. Both the high data rate and the complicated nature of the events require that each system be finely segmented. Thus the tracking, calorimetry, electron identification, and muon detection systems will each require of order 100,000-200,000 channels. For at least the calorimetry and tracking systems, the electronics must be low noise, fast, and operate at low power.

3. It does not seem to be feasible to form a trigger with significant rejection within the 16 nsec between beam crossings. Rather, estimates indicate that of order 500-1000 nsec will be required to form the initial, or level 1, triggers. It will therefore be necessary to delay, or pipeline, all information from the detectors. Information crucial to further triggers is digitized during the level 1 trigger processing.

4. Following the initial trigger system which will pass events at a rate of $10^4 - 10^5$ per second, a level 2 trigger system, utilizing primarily special purpose processors, will achieve a further rejection of events of approximately 100:1. Events passing the level 1 system should be buffered so that fluctuations in the initial pass rate do not lead to deadtime and loss of efficiency. For events passing the level 2 system, a matrix of scanners and ADC's will digitize the date for all channels containing information relevant to that event

5. Finally, a third level of decision-making will be performed using general purpose processors capable of reasonably complete and sophisticated reconstruction of events.

The general flow of the electronics summarized in Figure 21 has been discussed in several previous workshops[35,36]. In addition, it is to a large extent modeled after existing experiments such as UA1, UA2, CDF, and D0. It is encouraging to note that the performance required at each stage has been obtained, or is likely to be obtained, in existing experiments. Thus, for example, UA1 and UA2 have obtained rejections exceeding 1000 in the equivalent of a level 1 system for triggers on electrons, muons, and jets. CDF fully anticipates that its level 2 and level 3 system will achieve a combined rejection exceeding 10^4 That the total rejection of nearly 10^8 may be obtained remains to be demonstrated, however, since the selection criteria of the UA1-UA2 "level 1" systems are strongly correlated with those planned for level 2 - level 3 in CDF. For one process of great interest, $H^o \rightarrow W^+W^- \rightarrow e\bar{\nu}q\bar{q}$, a study[37] indicated that it should be feasible to attain the desired factor. For many of the other processes of interest, further work is required to demonstrate that the overall rejection can be achieved.

While all aspects of the electronics, trigger, and data acquisition system require significant development, it is apparent that the most serious technological challenges involve the front end electronics. Also, the design of the preamplifiers, amplifiers, etc. is very closely linked with the design of the detectors. For these reasons, and also because an earlier workshop at Fermilab concentrated on triggering and data acquisition[35], the Electronics group decided to focus attention primarily on the front end electronics. Of the many different types of front end systems, including among others those for tracking, calorimetry, muon detection, transition radiation detectors, etc., it was decided to concentrate on calorimetry and tracking both because these systems are in a sense the most basic and also because it was felt that solutions to problems in these areas would very likely be applicable to systems for other detectors.

Some discussion of level 1 triggering is also presented below; the reader is referred to the Electronics Group report[17] and to reference 35 for additional details on the level 2, level 3 triggering and the data acquisition systems.

Calorimeter Electronics

Schematic Diagram, Pulse Shaping, and Noise A schematic diagram of the electronics for the calorimeter is shown in Figure 22. It has already been noted in the section on calorimetry that it is desirable to use transformer matching for those channels with large source capacitance, and that short cables must be utilized if the risetime of the signal is to be kept as small as possible.

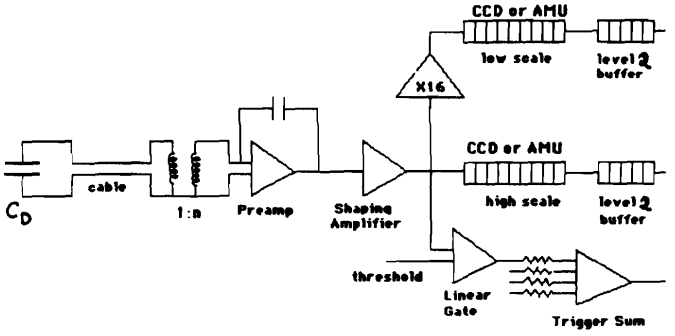

Figure 22
Schematic diagram of the front end electronics for the calorimeter. The output of the shaping amplifier is sampled and stored at 30 or 60 MHz in a CCD or analog memory unit (AMU).

The rather slow response produced by the inherent drift time in the liquid argon or by the slow risetime due to cables and preamplifier may be compensated to some extent by fast pulse shaping (with a corresponding decrease in the signal-to-noise). This is illustrated in Figures 23a - 23c which show the performance measured for the NA34 system.[13] Figure 23a shows the response of the preamplifier to a delta function charge injection (with the source capacitance attached), Figure 23b shows the response of the preamplifier to liquid argon signals, and Figure 23c shows the response after bipolar shaping. The peak of the signal, which is proportional to the energy deposition, is attained after 100 nsec. The time of the signal may be determined rather accurately from the zero crossing point.

For the particular geometry of the calorimeter considered during this workshop, the total source capacitance, equivalent noise charge, equivalent noise energy, event pileup noise, risetime, and time resolution were estimated. These results are presented in Table 2 and a discussion of the assumptions employed in their determination is included in the report of the Electronics Group.

Energy Measurement and Analog Pipeline The front-end circuitry following the shaping amplifier (which may produce either unipolar or bipolar signals) must perform at least the following functions:

1. energy measurement, via sampling of the voltage at the appropriate time
2. time measurement for at least the trigger towers, and preferably all towers
3. storage or delay of the analog information until the level 1 trigger is completed (0.5- 1 usec)
4. buffering of the information from events that have passed the level 1 trigger so that additional events may be recorded in a deadtimeless way.

These goals may be accomplished in a number of ways. In one of the simplest schemes the delay could be provided by a conventional delay line and the energy determined by two sequential samplings, one before the event of interest and one after the event of interest (suitably delayed to allow for the risetime).

In a high rate environment where the signals cover a large dynamic range, it is generally accepted that two samples are not sufficient; it is necessary to measure the slope of the baseline as well as its magnitude. This is then equivalent to "bipolar shaping". In addition, it will be essential to measure the time of energy depositions in at least the trigger towers. Because time invariant bipolar shaping is a natural choice for time measurement (the zero-crossing time is independent of the amplitude) and because the zero-crossing time may be easily and accurately measured by additional voltage samples, the analog pipeline or "analog ring buffer" shown in Figure 22 seems a natural choice. It combines the features of multiple voltage samples for energy and time determination, storage of the information during the level 1 trigger processing, and buffering of the information so that the system is deadtimeless. The actual technology and design that will be optimal to implement such an analog pipeline is not completely clear at this time. It can probably be accomplished with appropriate CCD's or with switched capacitor arrays such as the Microstore recently designed for use with the SLD detector[38].

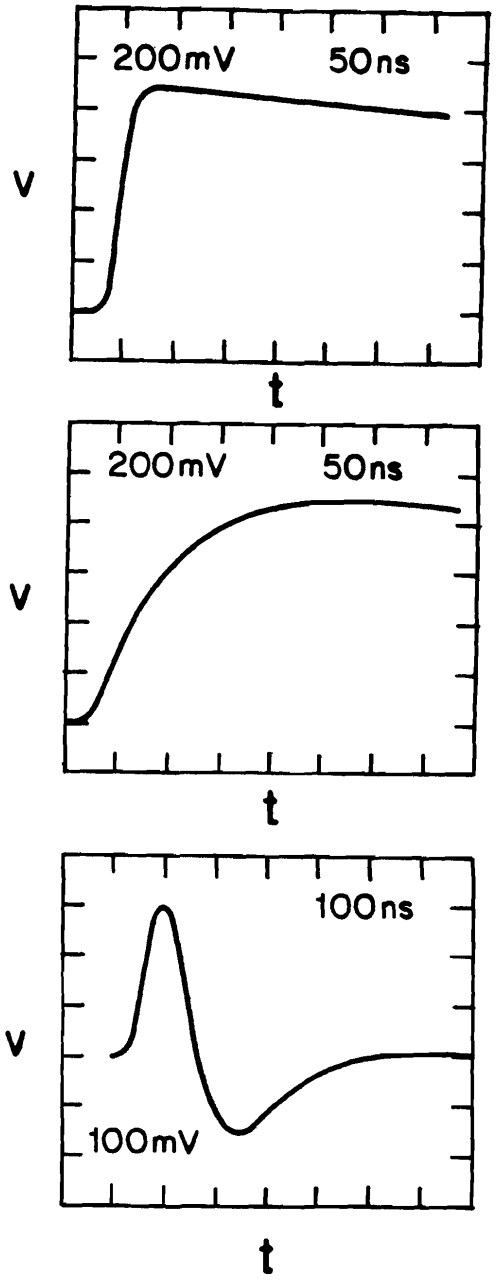

Figure 23
Measured response of the NA34 liquid argon calorimeter system. (a) Output preamplifier for δ function charge input. (b) Output of preamplifier for liquid argon signal. (c) Output of fast shaping amplifier for liquid argon signal.

Dynamic Range The dynamic range of the system is set by the maximum energy that must be measured without saturation and by the precision that is required at low energies. The most stringent criteria at the upper end of the scale is probably set by the search for Z bosons with masses in the

range 4 - 6 TeV; this implies that one must be able to measure energies of order 2 TeV in a single channel. At the low end, the inherent resolution of 12 - 15%/$\sqrt{E}$ for the electromagnetic calorimeter implies a resolution of 120-150 MeV at 1 GeV. One does not want to compromise this resolution since it is likely to be important for the determination of the position of electron showers. A scale of 100 MeV per channel is consistent with this; at the same time the inherent limitations due to electronic noise, uranium noise, and event pileup will probably prevent any substantial benefit from a finer scale. Hence the dynamic range of the system must be of order 14 bits.

Current systems, such as that for the CDF calorimetry, have demonstrated the feasibility of obtaining dynamic ranges equivalent to 16 bits in a relatively straight-forward and inexpensive way. While the preamplifier incorporates the full dynamic range, it is often simpler and less expensive to divide the signal at some point such that two parallel, overlapping systems of lesser dynamic range are utilized to accomplish the overall objective. Since the linearity of CCD's and simple switched-capacitor arrays is currently rather far from 14 bit performance, two parallel systems were assumed, each of 9-10 bit accuracy, as shown in Figure 22.

Track Chamber Electronics

The potential problems for track chambers of event pileup, distortion of the gain and drift velocity due to the equilibrium level of ions, and radiation damage are alleviated primarily by choosing small cell sizes and operation at low gas gain. Thus to a large extent the problems of tracking become identified with the challenge of developing an electronics system which simultaneously satisfies the requirements of low noise, low power, and high speed.

Types of Systems There will exist, of course, many different types of tracking detectors and readout which are optimized for different purposes, for example central tracking, intermediate angle tracking, forward tracking, transition radiation detectors, and microvertex detectors. There are at least three different types of electronics systems that may be utilized depending on the quantity which it is desired to measure. These include

1. Measurement of the total charge (or a fixed fraction of the total charge) deposited by individual particles
2. Measurement of the time of the signal from individual particles.
3. Measurement of the charge, as a function of time, resulting from one or more particles (waveform sampling).

It may be desired to make these measurements either on the signals induced on the wires (anodes) or on the cathodes.

It is important to distinguish between the requirements of (1), in which only one charge is measured per particle, and the rate of measurement is set by the instantaneous rate of particles (typically 3-6 Mhz) and the beam crossing rate (60MHz), and (3) in which multiple measurements of charge from a single particle are made either to obtain good timing resolution or to separate the charge distributions from different particles with spacing as close as 20 nsec. The latter system, which is often referred to as waveform sampling, typically requires frequencies of at least 100 MHz and preferably 200 MHz.

As noted earlier, the very high particle flux and questions of radiation damage, appear to require that a large part of the track chamber system use small cells, of either square, circular, or hexagonal geometry. The geometry of these cells is such that the positions of tracks will probably be determined by leading edge timing. In addition, there is little to be gained in attempting to resolve multiple tracks from the same event in a single cell, since the track separation in time is of the same order as the time during which the ionization is collected from a single particle. The Electronics group therefore decided to concentrate on systems of type (2) since a large fraction of the tracking electronics will be of this type and since it seems more likely that electronics of this type might be incorporated directly on, or very near to, the chamber itself.

Schematic Diagram, Pulse Shaping, and Performance A schematic diagram of a system for measuring the drift time for most track chambers is presented in Figure 24. If it is not to limit the performance of the tracking system, it must satisfy the following goals:

1. Sufficiently low noise to allow operation with gas gain of order 1-2 $\times 10^4$
2. Time resolution $\sim$1 nsec.
3. Double pulse resolution of 20-30 nsec

Fortunately, the continuing evolution and refinement of preamplifiers and amplifiers[22] has led to systems which are capable of the performance represented by (1) -(3). Of particular interest has been the development of rather simple, yet fast, shaping amplifiers capable of producing pulses of FWHM $\approx$ 6 nsec. The performance of one such system which utilizes delay-line clipping to suppress the exponential tail of the preamplifier and pole zero cancellation to nearly eliminate the 1/t falloff of the current pulse from the chamber is presented in Figures 25a - 25c. A four-fold integration with time constant $\approx$ 1 nsec is utilized as an approximation to gaussian shaping. These results were obtained with a very small chamber, but even for relatively large chambers it should be possible to obtain pulses with FWHM $\approx$ 12-15 nsec.

Power In addition to providing the performance discussed above, it is very important that the entire system-preamplifier, amplifier, discriminator, and time measurement- should con-

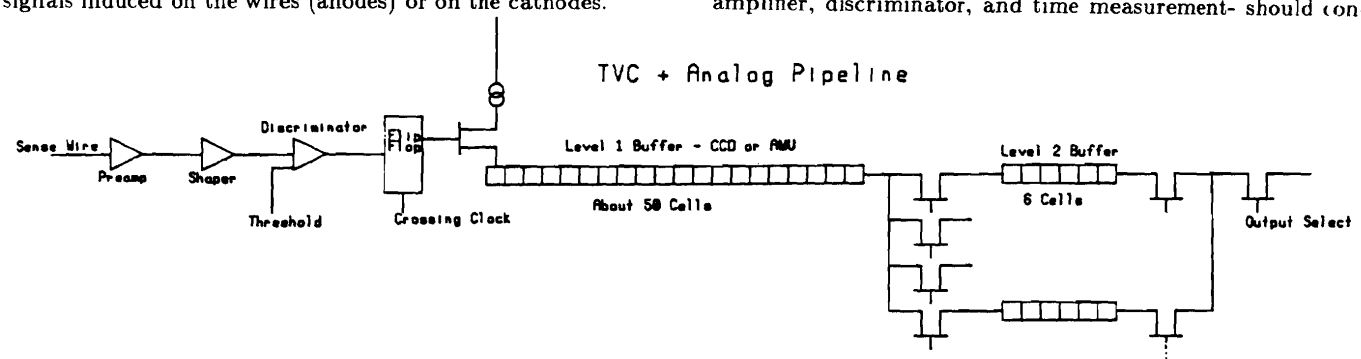

Figure 24
Conceptual design of the electronics for measuring drift times in a track chamber. In addition to a preamplifier, shaping amplifier, and discriminator, the circuit schematically shows time-to-voltage conversion followed by an analog buffer.

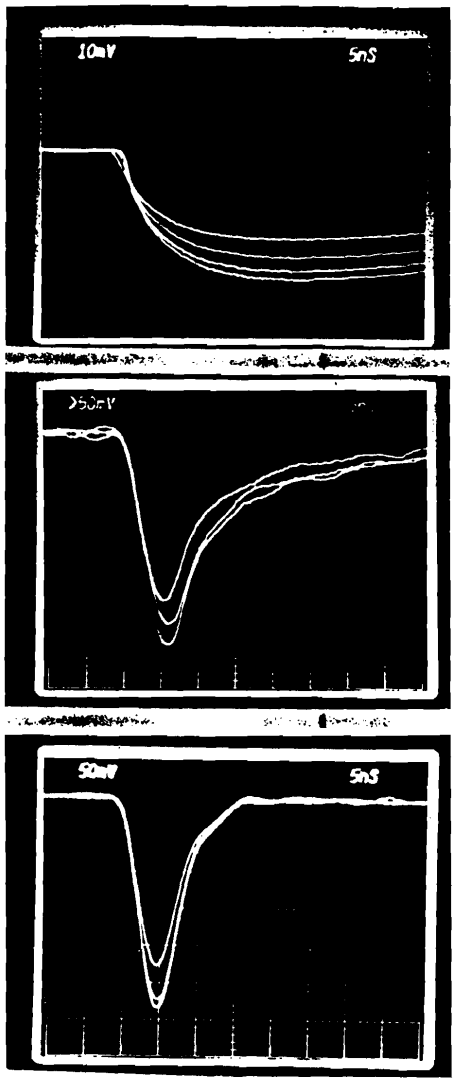

Figure 25
Response of track chamber electronics. (a) Preamplifier output. (b) Preamplifier tail cancelled (≈ anode current) (c) Anode current tail cancelled.

sume less than 100 mW of power. The motivation for such a low power is partially economic since the cost of crates, cooling, power supplies, etc. is to a large extent proportional to the total power. But the strongest motivation is provided by the desire to locate the entire front-end electronics system, up through the time measurment and digital or analog pipeline, directly on or very near to the chamber itself. The alternative, which is to route 50,000-100,000 cables to electronics at a remote location (even if remote is only 5 m distance) appears to be difficult to accomplish without seriously degrading the hermeticity of the calorimetry. It was felt that careful consideration of system design and redundancy would yield a system that was sufficiently reliable.

Time Measurement Two different systems were considered for time measurement. The first, schematically illustrated in Figure 24, uses time-to-voltage conversion and an analog pipeline. A pulse from a wire, if it exceeds the discriminator threshold, turns on a current source, which is then turned off by a subsequent pulse from a reference clock system. It is presumed that the reference clock would be synchronized with the crossing frequency and would run at 30 or 60 MHz. The goal would be to obtain a time resolution, at least in the absence of slewing or "walk" effects, of 200-300 picoseconds and full scale range of 30 - 60 nsec. Numerous such systems have been built using discrete components and there is no fundamental reason why such performance could not be obtained with fully integrated, or largely integrated, systems. The required dynamic range of the analog memory or analog pipeline would then be 8-9 bits.

A purely digital system for time measurement was also proposed and is discussed in detail in a contributed paper.[39]

Level 1 Triggers

One of the important assumptions in the trigger systems that have been proposed is that one can obtain a rejection factor of 10^3 10^4 within 0.5 - 1 usec. The Level 1 triggers that are typically regarded as crucial for selecting the events of interest are

1. Total E_t and missing p_t
2. Jets with $E_t > 40$ GeV
3. Isolated electrons with $E_t > 25$ GeV
4. Muons with $p_t > 10$ - 15 GeV

A fifth category which is more often listed among the level 2 triggers, but which is a candidate to be included in level 1, is that of high p_t tracks.

Trigger Times and Pipelining As indicated by the calculations on time resolution for the calorimeter, it should be possible to uniquely associate an energy deposition in a particular trigger tower with a particular beam crossing, if the energy deposition is sufficiently large to be important for the level 1 trigger. Since it is necessary in any event to have a one-to-one correspondance between a particular trigger and the raw data corresponding to that trigger, and since it may be useful even at level 1 to combine trigger information from different detectors, it is presumed that the output of any trigger system will have a time associated with it which allows that trigger to be uniquely identified with a particular crossing. If analog memory units or shift registers are used to pipeline the trigger information in the same manner as for the raw data, it should be straightforward to form combinations of triggers in a manner that is deadtimeless.

Calorimeter Triggers The calorimeter information will be extremely important for triggering and will be used to implement categories (1) - (3) above. These triggers require that one be able to multiply the energy in each tower, or sums of several trigger towers, by $\sin\theta \sin\phi$ or $\cos\phi$. Given the pipelined structure, it should be possible to accomplish this either with multiplying DAC's or with digital multipliers, and still be able to keep the association of each trigger with a particular crossing.

It has been found useful, both in offline analyses and in the formation of triggers, to exclude from energy sums those towers whose energy is below a certain minimum. This will be particularly important in the present high rate environment due to the significant amount of low energy noise which arises both from pileup and from electronic noise. Simple analog switches, such as that illustrated schematically in Figure 26, can be utilized to pass linearly the signal if it exceeds a certain threshold. It

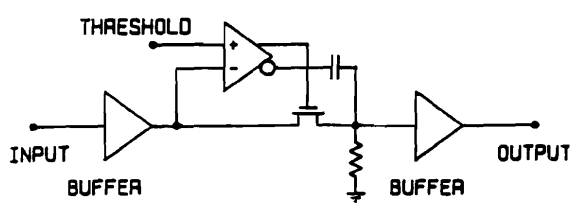

Figure 26
Analog gate with threshold.

is likely that such a switch will be utilized for each 0.06×0.06 trigger tower, though it is conceivable that direct analog sums of 2 - 4 towers might be performed first if coarser segmentation proves to be adequate.

Both the electron triggers and the jet triggers will require some form of crude clustering at level 1; the UA1 and UA2 experiments also found it important to include this capability so that prototype systems exist. For the electron trigger the clustering may simply be the sum of four adjacent towers. In order to obtain full efficiency, one must allow for energy sharing between trigger towers: hence each four-tower sum will presumably be offset from the adjacent sums by one trigger tower width (0.06×0.06). This is the scheme used very effectively by the UA2 experiment.

For the jet trigger, a similar technique might be utilized though one would sum all those trigger towers over a region of order $\Delta\eta \times \Delta\phi \approx 1 \times 1$. As with the electron trigger, such sums would have to be overlapping to attain full efficiency. It is also possible that more sophisticated algorithms may be developed that are sufficiently fast.

Muon Triggers Considerable attention was given to the topic of muon triggers. Fig. 27 shows estimated rates for all particles, particles with $p_t > 5$ GeV, particles exiting the calorimeter, and particles exiting the muon iron. For angles greater than 15°, simply the requirement that there exists a track segment pointing to the vertex will reduce the interaction associated rate to the level required, and should be sufficient to eliminate background from noise and cosmic rays. Should additional discrimination be required, a cut on the angle of the segment (at least in the central region) can be used to increase the momentum cut.

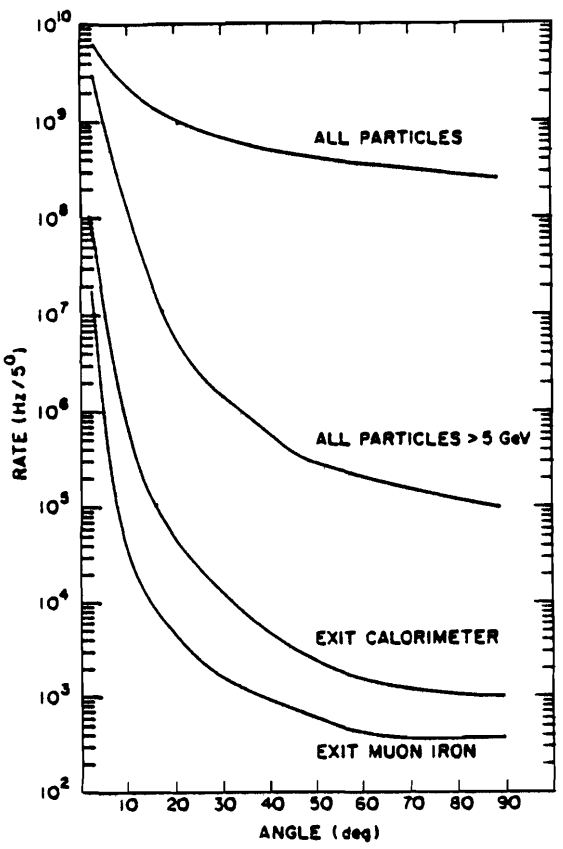

Figure 27
Raw angular rates for all particles, all particles greater than 5 GeV, all particles exiting the coarse calorimeter, and all particles exiting the muon iron.

In the forward direction, the rate of muons (both prompt and from decays) is sufficiently large that a reasonably accurate determination of momentum will be required at level 1; specifically, it will be necessary to impose a transverse momentum cut $p_t > 10$-15 GeV to reduce the trigger rate to acceptable levels. Since the displacement of a track from the infinite momentum trajectory for $p_t = 20$ GeV/c is small, e.g. 2.8 mm and 21 mm at polar angles of 0.77 and 5.7 degrees respectively, it will be necessary to use drift time information. A preliminary design of a track processor that performs a fast analog least-squares fit to the hit information was presented. The tower size corresponding to each track processor would be kept small enough to keep the rate in that trigger tower below 100 kHz in order to minimize ambiguities caused by multiple hits. To simplify the processor only hits from planes with low multiplicity would be utilized. A simulation of 1 TeV muons propagating in magnetically saturated iron was performed to study the effect of muon-induced electromagnetic showers; it was found that if five detector stations are used, each separated by 1 m steel, then at least three detector planes were clean for 97% of the events.

While further studies are clearly required, there was considerable optimism that it should be reasonably straightforward to design a muon level 1 trigger which would reduce the trigger rate to less than 10 kHz.

Forward and Other Specialized Detectors

While many of the participants pursued the Nirvana of a large 4π detector that is capable of doing all physics, a small group of enthusiasts[40] pursued detectors in the forward direction, spurred on by the observation that the rapidity interval 5-10 will in fact be undetected by the "4π" detectors. Inspiration for studying this region is provided by (1) the hope that there may be new physics that is preferentially produced in the forward direction and (2) the observation that final states with masses in the several hundred GeV range are produced with equal rates in each unit of rapidity and may in some instances be better studied (for example with superior particle identification) in the forward region.

Several different geometries were considered. In one (Figure 28), originally proposed by Bjorken[41], quadrupole spectrometers, including particle tracking, calorimetry (and optionally ring imaging cerenkov counters) are spaced along two kilometers thereby allowing coverage over nearly the full rapidity range.

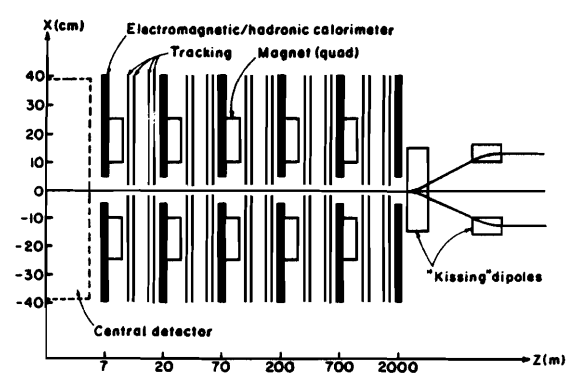

Figure 28

Schematic illustration of forward detector proposed by Bjorken.

A more traditional approach[40] led to the layout shown in Figure 29. The spectrometers were designed to allow study of forward production of states in the mass region $\lesssim$ 1.6 TeV; the purpose is to preserve access to the range of CM energy available at the Tevatron, while taking advantage of different kinematics in order to improve the quality of the measurement. Three spectrometers, each containing track chambers, ring imaging cerenkov counters, calorimetry, and muon detectors, were used to cover the angular interval 0.2 - 200 mrad.

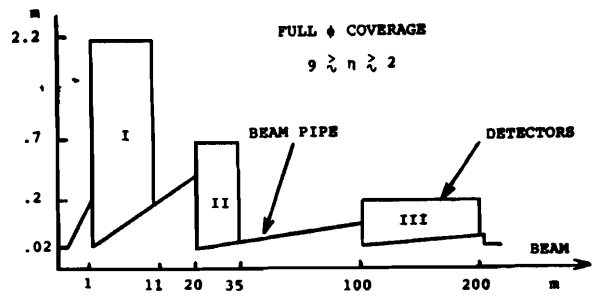

Figure 29
Schematic of a more conventional forward detector proposed by Schlein and Foley.

Still another design is that of the "Taster" which is illustrated in Figure 30 and discussed in detail in the report of the Heavy Quark group.[42] One of the primary goals in the design of this detector is that one be able to study rare B decays and CP violation. Even at the SSC B mesons will be produced primarily at low p_t. It is argued that the detection of leptons of several GeV transverse momentum is much easier in the forward direction where the momentum of such particles is of order 10-30 GeV rather than 2-5 GeV. In addition, charged particle identification, which is apt to be important in the ultimate B decay experiment, may be easier to implement in the forward direction.

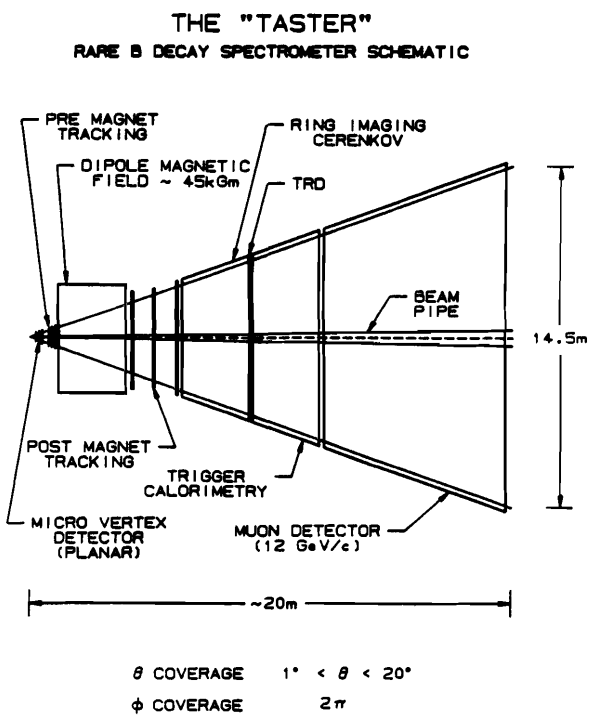

Figure 30
Schematic of the "Taster" detector which is designed primarily to study B decays.

A detector design for scattering in the very forward region, in particular for small angle elastic scattering, was put forth by DeSalvo, Orear, and Maleyran.[43] They conclude that by using thin walled proportional tubes inserted directly into the beam pipe, it should be possible to measure elastic scattering to angles as small as 10^{-6} radians, the region in which Coulomb scattering dominates.

DETECTOR SIMULATION

It is widely recognized that to make further progress in the design of calorimeters, track detectors, and the overall detector design, more sophisticated and accurate simulations will have to be performed. Such simulations pose a formidable task and will in all likelihood require a concerted effort on the part of a number of individuals. Motivated by this need, Price and Lebrun spontaneously formed an ad hoc working group on detector simulation during the workshop. Their report[44] reviews the currently available programs for detector simulation and discusses the requirements for SSC. The group also makes recommendations on how to proceed in order to most effectively accomplish the desired goals.

CONCLUSION

One of the challenges presented to the participants at the beginning of the workshop was that of examining each of the major detector systems in considerably greater detail than had been done in previous workshops, with the goal of understanding whether it is in fact *feasible* to build a detector such as outlined in the DCMAP report or in the Proceedings of Snowmass 84. The suggestion that one think about such mundane problems as mechanical structure, power dissipation, electrostatic stability of wires, cable routing, etc. prompted a few good-natured remarks that it is unheard-of that one should do "honest work" during a summer study; however, most of the groups rose to the challenge and made considerable progress towards this goal. In addition, this workshop benefited enormously from progress made in the development of detectors and electronics in the last two years. While a number of questions remain to be answered, it seems clear that it will be possible to build detectors which accomplish most of the goals outlined in the Introduction and which will allow one to effectively address the physics potential of the SSC.

A second charge to the working groups was that they attempt to identify areas of research and development that seemed to be particularly important for implementation of the detectors being considered. While the Task Force on Detector R & D for the SSC has already produced an excellent report on this subject, it seemed useful to ask the participants of the workshop to also focus on it. They did so and clearly identified a number of areas which they felt to be particularly important. Happily, and not surprisingly, there is a large overlap with the recommendations of the Task Force.

It is interesting to note that much of the R & D during the last two years that is most relevant to SSC detectors was carried out not for the SSC but for the sake of other experiments. For a variety of reasons, including the fact that nearly all of the major colliding beams detectors are no longer in the R & D phase, and that the particular problems for the SSC of high rate and radiation hardness are not always shared by other experiments, it is unlikely that one will be able to rely on this mechanism in the future. It is important that an aggressive R & D program focussed on the problems posed by detectors at high luminosity, high energy colliders be initiated as soon as possible.

ACKNOWLEDGEMENTS

Needless to say a very large amount of effort is required to make a workshop such as this one a success. Lee Pondrom had the courage to take on the task of the overall organization. Special thanks to Joanne Day and her staff for their untiring efforts, both before and during the workshop, to make it happen and run smoothly. Robin Craven once again miraculously transformed empty condominiums into a productive computer center.

I would also like to thank the working group leaders who were willing to steal time from their busy schedules and upset their summer plans in order to organize and lead the individual groups; in every instance they did an outstanding job.

Special recognition goes to Veljko Radeka and Sergio Rescia for their valuable contributions to the workshop and for the many conversations I have had with them.

Finally I would like to thank Christine Feinberg for patiently preparing this report and Rene Donaldson for her efforts (and patience) in putting the entire Proceedings together.

REFERENCES

1. Proceedings of the 1984 Summer Study on the Design and Utilization of the Superconducting Collider, edited by R. Donaldson & J.G. Morfin, Snowmass, CO. (1984). This work is referred to in subsequent references as Snowmass 84.
2. Proceedings of the ECFA-CERN Workshop on a Large Hadron Collider in the LEP Tunnel. CERN Report 84-10.
3. Cost Estimate of Initial SSC Experimental Equipment, SSC-SR-1023, June 1986.
4. D. Theriot et. al., *4 pi Detectors*, these Proceedings.
5. H. Gordon and P. Grannis, *Calorimetry for the SSC*, Snowmass 84, 541.
6. T. Kondo and K. Niwa, *Electromagnetic Shower Size & Containment at High Energies*, Snowmass 84, 559.
7. R. Partridge, *Calorimeter Requirements for Tagging the Semileptonic Decays of Top Quarks*, Snowmass 84, 567.
8. E. Fernandez et al, *Identification of W Pairs at the SSC*, Snowmass 84, 107.
9. P. Grannis et al, *Identification of Electrons at the SSC*, these Proceedings.
10. C. Baltay, J. Huston, and B. Pope, *Calorimetry for SSC Detectors*, these Proceedings.
11. ALEPH Technical Proposal, CERN, Geneva, Switzerland.
12. The parameters of the calorimeter assumed by different working groups are not always identical. These parameters are in any event approximate and the variations in assumptions should not be of any consequence.
13. NA34 experiment, CERN
14. D0 Design Report, Fermilab.
15. SLD Design Report, SLAC.
16. V. Radeka, Academic Training Lectures at CERN. These lectures were also presented during the workshop.
17. T. Devlin, A. Lankford, and H. H. Williams, *Electronics, Triggering and Data Acquisition for SSC Detectors*, these Proceedings.

17a. A. Yamashita and K. Kondo, *Physics Noise to Calorimetry at SSC*, these Proceedings.

18. H. Iwasaki, B. Milliken, S. Protopopescu, and R. Raja, *Hermeticity Studies in SSC Type Calorimeters*, these Proceedings.
19. G. O. Alverson and J. Huston, *Estimation of Background Noise in LAr Detectors Due to Pileup*, these Proceedings.
20. D. G. Cassel and G. G. Hanson, *Report of the Central Tracking Group*, these Proceedings.
21. M. Atac, *Wire Chamber Aging*, Proceedings of the Workshop on Radiation Damage to Wire Chambers, LBL Report 21170.
22. J. Fischer, A. Hrisoho, V. Radeka, P. Rehak, Nucl. Instrum. Methods **A238**, 249 (1985).
23. Research on CF_4 and other candidates for a faster gas is under way at Heidelberg, A. Wagner, private communication.
24. R. Desalvo, *A Proposal for an SSC Central Tracking Detector*, these Proceedings; A. Odian, *A Variation on the Straw Chamber Theme for the Central SSC Drift Chamber*, these Proceedings. R. Palmer suggested using straws for a central track detector for Isabelle in 1980.
25. J. Carr and H. Kagan, *Wire Stability Studies for an SSC Central Drift Tracker*, these Proceedings.
26. K. Lane and J. Rohlf, *Top Quark Identification through Isolated Energetic Leptons*, Snowmass 84, 737.
27. J. Carr and E. Eichten, *Lepton Identificaton at the SSC*, Snowmass 84, 703.
28. For a summary of the e/pi rejection ratio obtained with calorimeters in previous tests, see the Report of the Task Force on Detector R&D for the SSC, SSC-SR-1021, p. 178.
29. Y. Fukui et al, *e/pi Separation in the CDF End Plug EM and Hadron Calorimeters*, these Proceedings.
30. Proposal for UA2 upgrade, CERN
31. R. Bouclier et al, IEEE Trans. Nucl. Sci. **33**, 169 (1986)
32. R. Engelmann et al, Nucl. Inst. Methods **216**, 45 (1983)
33. D. Carlsmith et al, *SSC Muon Detector Report*, these Proceedings.
34. B. Adeva, *New Z Boson Physics with a Specialized Muon Detector of the L3 Type at the Supercollider*, these Proceedings.
35. Proceedings of the Workshop on Triggering, Data Acquisition and Computing for High Energy/High Luminosity Hadron-Hadron Colliders, 1985, ed. B. Cox, R. Fenner, and P. Hale, Fermilab, Batavia, Illinois. (Trigger 85)
36. Proceedings of the DPF Workshop on Collider Detectors: Present Capabilities and Future Possibilities, Lawrence Berkeley Laboratory, 1983, ed. Stewart C. Loken and Peter Nemethy.
37. M. Abolins et al, *Report of the High Level Group*, Trigger 85, 131.
38. G. M. Haller, D. R. Freytag, J. T. Walker, and S. I. Chae, IEEE Trans. Nucl. Sci. **NS-33**, 221 (1986); D. R. Freytag and J. T. Walker, IEEE Trans. Nucl. Sci. **NS-32**, 622 (1985).
39. Y. Arai and T. Ohsugi, *An Idea of Deadtimeless Readout System by using Time Memory Cell*, these Proceedings.
40. E. Courant et al, *Summary, Small Angle Spectrometers*, these Proceedings.
41. J. D. Bjorken, *Forward Spectrometers at the SSC*, Fermilab-Conf-86/22
42. B. Cox et al, *Report of the Heavy Quark Group*, these Proceedings.
43. Lawrence E. Price and Paul Lebrun, *Report of the Working Group on Detector Simulation*, these Proceedings.